Modeling of Small-Scale Wind Energy Conversion Systems

Bridget Erin Buehrle

Thesis submitted to the faculty of the Virginia Polytechnic Institute and State University
in partial fulfillment of the requirements for the degree of

Master of Science
In
Mechanical Engineering

Shashank Priya, Committee Chair
Danesh K. Tafti
Walter F. O'Brien

May 8, 2013
Blacksburg, VA

Keywords: small-scale, wind, diffuser, vertical axis, tubercle

Modeling of Small-Scale Wind Energy Conversion Systems

Bridget Erin Buehrle

ABSTRACT

As wind turbines are increasingly being adopted for meeting growing energy needs, their implementation for personal home use in the near future is imminent. There are very few studies conducted on small-scale turbines in the one to two meter diameter range because the power generated at this scale is currently not sufficient to justify the cost of installation and maintenance. The problem is further complicated by the fact that these turbines are normally mounted at low altitudes and thus there is necessity to have the optimum operating regime in the wind speed range of 3-10 mph (1.34 – 4.47 m/s). This thesis discusses two methods for increasing the efficiency of horizontal axis small-scale wind energy conversion systems, 1) adding a diffuser to increase the wind speed at the rotor and 2) designing tubercles to enhance the flow characteristics over blades. Further, it was identified during the course of thesis that for simple installation and maintenance in the residential areas vertical axis turbines are advantageous. Thus, the second chapter of this thesis addresses the design of vertical axis turbines with power generation capability suitable for that of a typical US household.

The study of the diffuser augmented wind turbine provides optimum dimensions for achieving high power density that can address the challenges associated with small scale wind energy systems; these challenges are to achieve a lower start-up speed and low wind speed operation. The diffuser design was modeled using commercial computational fluid dynamics code. Two-dimensional modeling using actuator disk theory was used to optimize the diffuser design. A statistical study was then conducted to reduce the

computational time by selecting a descriptive set of models to simulate and characterize relevant parameters' effects instead of checking all the possible combinations of input parameters. Individual dimensions were incorporated into JMP® software and randomized to design the experiment. The results of the JMP® analysis are discussed in this paper. Consistent with the literature, a long outlet section with length one to three times the diameter coupled with a sharp angled inlet was found to provide the highest amplification for a wind turbine diffuser.

The second study consisted of analyzing the capabilities of a small-scale vertical axis wind turbine. The turbine consisted of six blades of extruded aluminum NACA 0018 airfoils of 0.08732 m (3.44 in) in chord length. Small-scale wind turbines often operate at Reynolds numbers less than 200,000, and issues in modeling their flow characteristics are discussed throughout this thesis. After finding an appropriate modeling technique, it was found that the vertical axis wind turbine requires more accurate turbulence models to appropriately discover its performance capabilities.

The use of tubercles on aerodynamic blades has been found to delay stall angle and increase the aerodynamic efficiency. Models of 440 mm (17.33 in) blades with and without tubercles were fabricated in Virginia Tech's Center for Energy Harvesting Materials and Systems (CEHMS) laboratory. Comparative analysis using three dimensional models of the blades with and without the tubercles will be required to determine whether the tubercle technology does, in fact, delays the stall. Further computational and experimental testing is necessary, but preliminary results indicate a 2% increase in power coefficient when tubercles are present on the blades.

Acknowledgements

I would like to thank my advisor Dr. Shashank Priya, and my committee members Dr. Danesh Tafti and Dr. Walter O'Brien for their support and guidance throughout my graduate career. I would also like to thank my colleagues Ravi Kishore and Colin Stewart for their consultation and help while I simulated models using computational fluid dynamics. I am grateful to God and my family and friends for the support that has helped me reach my goals. I am very appreciative of my parents, Ralph and Barbara, my brothers, Joe and Blaine, and my fiancé Brent, for encouraging me throughout my master's and for always believing in me.

TABLE OF CONTENTS

LIST OF FIGURES

LIST OF TABLES

LIST OF SYMBOLS

2D: two-dimensional

3D: three-dimensional

α: angle of attack

A_o: swept area of diffuser augmented wind turbine

A_1: swept area of the turbine a rotor the size of the largest diameter of the diffuser augmented wind turbine

C: airfoil chord length

C_D: drag coefficient

C_L: lift coefficient

C_P: power coefficient

C_{pres}: pressure coefficient

D: diameter of rotor

γ_{pu}: fraction of time the flow moves downstream

h: height of diffuser flange

H: height of airfoil

L: length of diffuser

λ: tip speed ratio

L_{in}: diffuser inlet length

L_{out}: diffuser outlet length

η: overall efficiency of turbine

p_1: pressure at the inlet of the diffuser

p_2: pressure at the outlet of the diffuser

P: power

P_o: power from the diffuser augmented wind turbine

P_1: power from the bare wind turbine of largest DAWT diameter

R: vertical axis wind turbine radius

r: radius of diffuser augmented wind turbine rotor

ρ: density of air (wind)

Re: Reynolds number

σ: solidity

θ_{in}: diffuser inlet angle

θ_{out}: diffuser outlet angle

T: torque

U_o: wind velocity at turbine blades

U_∞: inlet wind velocity

ω: angular velocity

LIST OF ACRONYMS

CFD: computational fluid dynamics

D: detached

DAWT: diffuser augmented wind turbine

DES: Detached Eddy Simulation

ID: incipient detachment

ITD: intermittent transitory detachment

HAWT: horizontal axis wind turbine

LES: Large Eddy Simulation

RANS: Reynolds Averaged Navier Stokes

TD: transitory detachment

VAWT: vertical axis wind turbine

1. INTRODUCTION

The emphasis on using renewable energy sources is growing rapidly as the prices of many fossil fuels continue to be volatile and the repercussions of not addressing and not mitigating carbon dioxide emissions becomes more impactful on the environment. The global population is continuing to increase, and with that comes more energy consumption. Additionally, as countries develop, they tend to use more energy per capita. In general, more energy use means more carbon dioxide emissions. Thus, it is important to find pathway to meet the worlds' energy needs without drastically changing the population's energy-use habits (1). The application and commercialization of small-scale wind energy can provide sustainable clean energy a viable option for constituents of both developing and developed countries while contributing towards the reduction of carbon dioxide emissions. Since the use of wind energy can allow for the decrease of the use of fossil fuels, wind energy will lower harmful emissions because it decreases the use of "dirtier" fuels (2). It was found that if 20% of the United States energy were from wind power, it would reduce carbon dioxide emissions by 25% compared to the emissions of our baseline energy mix (2).

The use of wind turbines increases the potential for a more environment friendly sustainable energy supply. However, there is still much development required before wind energy can become a popular high-output energy provider. Turbine performance enhancing features such as diffusers and tubercles for blades have been investigated in literature to evaluate their impact on our energy mix. Additionally, vertical axis wind turbines (VAWT) have been explored to determine whether they could provide user friendly technology that is simpler to install and maintain.

A diffuser can be used to increase the velocity of the wind flowing through the wind turbines' blades. This is especially important for smaller scale wind turbines that do not produce large enough amounts of energy to make them attractive in the market. The demand for small scale wind turbines (1 to 2 m (3.28-6.56 ft) diameter range) is currently rather low because of their low power output and high start-up speed. Diffusers can not only lower the start-up speed required for the turbine to begin producing electricity (3), but can also increase the velocity at the rotor, which increases the power output by the third power of velocity change. In this thesis, statistical analysis was used to find the optimum geometry for the wind turbine diffuser because it reduces the number of diffuser geometries that should be analyzed and elucidates the effects of individual parameters without testing each geometry in the wind tunnel. Statistics allows for a specified set of relevant geometries to be simulated using computational fluid dynamics (CFD) and optimized using statistical software. This reduces the computational cost and still provides the user comprehensive understanding of the effect of variety of geometrical parameters.

While horizontal axis wind turbines (HAWT) have been the major players in large-scale wind energy production, the inclusion of smaller vertical axis wind turbines may be able to increase the adoption of windmills in the residential domain. Traditionally horizontal axis wind turbines are used in wind farms and for large scale wind energy production. Recent research has found that VAWTs may be able to be spaced more closely together in a wind farm than HAWTs, and the closer spacing may even increase their efficiency (4). Another benefit of the VAWT design is that they start up at lower speeds and are naturally omnidirectional. The potential of VAWT for harnessing the

wind can be modeled first using CFD and then experimentally to verify its utility and limitations. The ability of the popularly used NACA 0018 airfoil was simulated in this thesis for a six-bladed vertical axis wind turbine.

New developments in bio-inspired technology can also impact the efficiency of wind turbines. Researchers have found that the addition of whale-like tubercles can delay stall on a blade (5). Using such a blade for small scale turbines (1-2 m (3.28-6.56 ft)) was explored in this thesis using three-dimensional analyses in CFD. Significant enhancements in aerodynamic efficiency can make small-scale wind energy a more viable option for the residential wind energy market. There is much to be learned from nature around us, and for this reason bio-inspired technologies are becoming an important research area. The ability to increase efficiency of horizontal and vertical axis wind turbines allows them to produce more power and makes them cost effective. By making small-scale wind energy more attractive both aesthetically and in its output, an increase in its use will occur on the residential-scale.

2. LITERATURE REVIEW

While large-scale wind energy usage has continually increased in recent years (6), there is still little to no use of residential-scale wind energy conversion systems. This is due to their high costs and low energy output. However, through the use of velocity enhancing devices such as wind turbine diffusers attached to horizontal axis wind turbines, residential-size wind energy can become a viable option. Amplifying the velocity through the turbine is important for increasing the power output because power is proportional to velocity cubed. Vertical axis wind turbines generally have a lower start up speed, simpler installation and reduced acoustic noise which makes them an attractive option for residential applications. Tubercles are another performance enhancing device that can improve the power output of wind turbine blades.

The chapters in this thesis address three important aspects of the wind turbine performance enhancing features. The wind turbine diffuser is a component added exterior to the wind turbine to amplify the wind velocity through the turbine's blades. Vertical axis wind turbines are a lesser used variety, and thus there is still more exploration to do in this area. Finally, the analysis of the effects of tubercles for a wind turbine blade allowed for reducing the stall on the turbine.

2.1 Residential-Scale Diffuser Augmented Wind Turbine

The work presented in this thesis uses actuator disk theory and computational fluid dynamics to model a variety of diffuser designs based on the lessons learned from previous literature (7, 8, 9, and 10). Sorensen et al. (7) introduced the actuator disk theory as an appropriate model for wind turbines in computational fluid dynamics. It was

pointed that for a rotor, the actuator disc is a permeable surface normal to the free stream velocity on which an even distribution of blade forces acts upon the flow (7). The Euler equations were discussed in detail in their work (7) along with the boundary conditions.

Ohya et al. found that a significant increase in wind speed was obtained if a long diffuser body over [greater than] L/D =3 is used (8), where L is the length of the diffuser and D is the diameter of the wind turbine. Ohya et al. also found an optimal ratio of outlet area to inlet area of 2.35 (8). It was pointed out that optimum flange configuration results in a low-pressure region in the exit neighborhood of the diffuser by vortex formation and draws more mass flow to the wind turbine inside the diffuser shroud (8). In their work, the optimal flange length was found to be h/D = 0.25, where h is the height of the flange and D is the turbine diameter. If the flange is larger than h/D = 0.25 then there is a pressure increase in the upstream flow in front of the diffuser and the incoming wind does not flow smoothly. Ohya et al. tested the effects of diffusers with large open angles and other variations in geometry and were able to achieve power augmentation factor of 4 to 5 times.

Salim et al. (9) have explained the function of using the wall y+ value to evaluate the accuracy of mesh size. They defined the wall y+ value as a non-dimensional distance similar to local Reynolds number given by the ratio between the turbulent and laminar influences in a cell (9). Bardina et al. have described the governing equations surrounding the motion of turbulent flow and quantified the suitability of various turbulence models including the k-ε and k-ω models. It was pointed out that the k-ε model provides good results for free-shear-layer flows with relatively small pressure gradients and requires explicit wall-damping functions and fine grid spacing near solid walls (11). The finding

that the k-ω model is superior in numerical stability as compared to the k-ε model in the viscous sub layer near the wall was decisive in utilizing it in this thesis (in its shear stress transport (SST) version). The results of Bardina et al. lead to the conclusion that the best overall model is the k-ω SST model that can predict complex flows involving separation.

It is very difficult to determine the correct turbulence model to use when modeling at low wind speeds. Muggli et al. have used the k-ε model even though it underestimates the blockage caused by the recirculation in the flow separation region and overestimates the pressure recovery in the diffuser (12). They found that although the Navier-Stokes code with the standard k-ε turbulence model is able to predict the presence of separation in the flow, it is not able to accurately predict the static pressure rise of highly loaded pump diffuser beyond the flow separation point (12). In support of using a different turbulence model, Muggli et al. stated that the simulations of the two-dimensional diffuser showed that current CFD methods with the k-ε turbulence model have extreme difficulty in predicting exact diffuser performance in regions where separation has occurred. Wang et al. validated the use of CFD to model the fluid flow through a turbine by comparing the analytical and experimental results (10). In their work, it was found that by using a scoop inlet, the power output increased by a factor of 2.2. CFD results in their analysis were found to be comparable to those from wind tunnel experiments. Simpson (13) has provided understanding of turbulent boundary layer separation which occurs due to the adverse pressure gradients around streamlined and bluff bodies. Further Simpson has detailed the nature of transitory stalls in diffusers (13). It was suggested that there is a lower limit to the 2θ angles that must be exploited to construct an effective diffuser with little separation. So, while the velocity of the air

flowing through the diffuser rises as the angle of the diffuser rises, the angle must be kept low else there is risk of separation.

2.2 Small-Scale Vertical Axis Wind Turbine

Vertical axis wind turbines (VAWT) are traditionally labeled as one of two types, Darrieus and Savonius. Savonius VAWTs are generally drag-based, simple machines that consist of scooping blades, while Darrieus types use an airfoil to generate electricity and can look more like eggbeaters. Figure 2.1 from Islam et al. (14) shows pictures of both types of vertical axis wind turbines. In this thesis, we have focused on the Darrieus type VAWT.

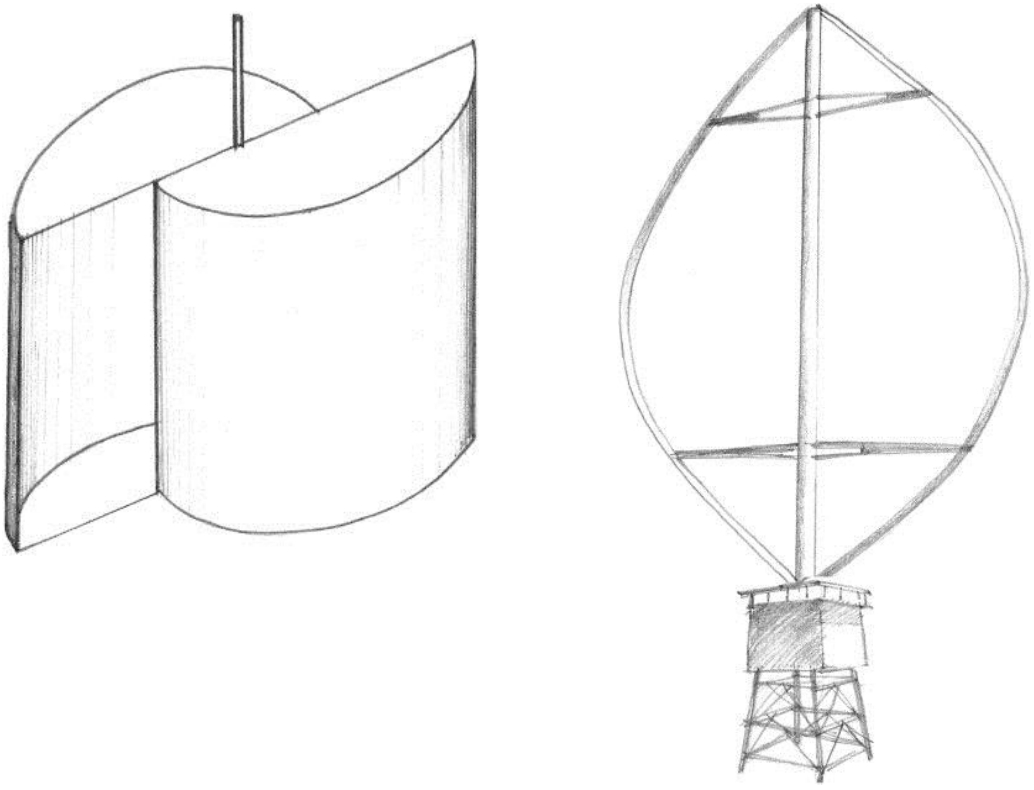

(a) (b)

Figure 2.1. Savonius (a) and Darrieus (b) vertical axis wind turbines. *Note:* Diagrams are from Islam et. al, 2008 (14).

While HAWTs are typically used for large-scale wind power generation, little attention has been given to VAWTs until recent years. Even though their power output has been reportedly lower than HAWTs in large scale applications (15), the VAWT design has many advantages. Vertical axis wind turbines can start-up at lower speeds than horizontal axis wind turbines of comparable size. Recent research by Whittlesey et al. asserts that VAWTs can also be placed more closely than HAWTs in a wind farm. It was pointed out that when HAWTs are closely spaced in wind turbine farms their power coefficients is reduced but VAWTs can be placed closely together and experience much smaller decreases, or, in some cases even an increase in power coefficients (4). The reason for this increase was proposed to be related to the aerodynamic interactions occurring between a pair of counter-rotating VAWTs (4). Dabiri has also made similar conclusions in his study (15). VAWTs can be more closely spaced because there are higher turbulence levels near the ground that increases the kinetic energy delivered to the turbines (15). The same is true for tidal turbines according to Antheaume et al. (16).

Through virtue of their design, VAWTs are naturally omni-directional, as opposed to HAWTs which can only work when they are facing the wind. VAWTs are also quieter than HAWTs and easier to maintain because components are closer to the ground (17). The disadvantages of VAWTs, and a main reason that they are less popular is the fact that they must be installed close to the ground and that they typically produce less energy than their horizontal counter(-rotating) parts.

One of the objectives in this thesis is to characterize a VAWT design that can contribute to the electricity mix in the future. To ensure that the VAWT models are

accurate, the first step was to validate the computational fluid dynamics models using a single airfoil. Sheldahl et al. (18) have performed wind tunnel experiments on various symmetrical airfoils at low Reynolds numbers to find the coefficients of lift and drag that may occur for vertical axis wind turbines. The data was extrapolated to include information for the NACA 0018 airfoil. Other researchers have used the NACA 0018 airfoil for vertical axis wind turbines and found that there is a low lift coefficient and high drag coefficient (19).

Two-dimensional modeling of vertical axis wind turbines has been proven to give accurate results. Untaroiu predicted VAWT operating speed with 12% error, but found that intermediate turbine performance is not accurately captured (20). Untaroiu and Howell et al. (50) have both discussed the abilities and shortcomings of 2D and 3D simulation for predicting VAWT performance. It was found that 2D simulation over predicts the performance while 3D simulation under predicts (with 20% computational error) (20). Further it was found that both 2D and 3D simulations become less reliable at higher tip speed ratio. The reason for discrepancy in 2D and 3D results was related to the failure to capture tip vortex shedding (20). One of the important conclusions made in the work of Untaroiu was that regardless of which turbulence model is chosen, the 3D approach does not exhibited significant advantage over 2D, rather it complicated the calculations. Hameed et al. (19) have also used 2D model for their analysis that saves computational time and simplifies the analysis.

Both Maître et al. (21) and Untaroiu (20) discuss the grid refinement studies used to validate the meshing of their models. Maître et al. found that y+ values under one are the best when the k-ω SST turbulence model is used (21). Untaroiu used y+ values as

high as 1.7 and still achieved results comparable to experimental data, but they used the k-ε model with scalable wall functions (20). In this thesis, a transition SST turbulence model was used in accordance with the findings of Maughmer et al. (22) and y+ values less than one were achieved.

2.3 Enhancement of the Flow Characteristics through Tubercles on a Wind Turbine Blade

One of the issues with small-scale wind energy is that it does not always generate enough electrical power to be economically viable. By exploring the mechanisms available in nature, researchers have been able to propose solutions for many challenging technical problems. Bio-inspired technologies and biomimetics are related to the use of principles found in nature to inspire a new technology or innovation. The concept of tubercles is derived from humpback whales, and their inclusion on to the turbine blade has been projected to delay stall and increase the efficiency. Whales use their tubercles to aid in movement and to capture their prey. The tubercles are effectively a leading-edge control device that maintains lift and delays stall until higher angles of attack (23). Since the goal of wind turbine airfoils (for lift-driven designs) is to maximize the lift-drag ratio on the blades (24), the use of tubercles can enhance the blade performance by maintaining the lift.

Van Nierop (5) has found that the bumps alter the pressure distribution on the wing such that separation of the boundary layer is delayed behind bumps. This ultimately leads to a gradual onset of stall and a larger stall angle (5). Fish et al. (23) support the findings of van Nierop (5) and have performed an experimental analysis of finite wing

models. They concluded that tubercles with amplitude of 4% of wing chord can significantly reduce the negative effect of the separation and fosters re-attachment (23). Important findings from their study includes a 4.8% increase in lift for blades with tubercles compared to those without, a 10.9% decrease in drag, and a 17.6% increase in lift/drag ratio when the angle of attack was 10˚ (23). These are important results for small-scale wind turbines because of the increase in lift and delay of stall. At higher Reynolds numbers the effectiveness of tubercles starts to disappear and they were found to not generate as much lift and even accelerate the onset of cavitation (23).

Miklosovic et al. have performed wind tunnel experiments comparing a scaled model of a humpback whale flipper to a similar model without tubercles. The results showed that the leading-edge tubercles delayed the stall angle by about 40% and increased the lift and drag (25). The maximum lift coefficient was shown to increase by 6% as compared to the smooth model, and there was a higher lift at higher incidence angles (25). A reason for the increased lift may be related to the trailing edge vortices. Swanson et al. found that blades with a smooth leading edge have trailing edge vortices that rotate in the same direction, but blades with tubercles on the leading edge have vortices that rotate in opposite directions, thus canceling out the trailing vortices which can contribute to a weaker tip vortex (26). This is an important development because Abbot found, while summarizing airfoil data in 1959, that trailing vortices reduce the slope of the lift curve (27). In 1959, they had not yet applied the addition of leading-edge tubercles to their airfoils, so they were only seeing the effects of vortices that rotated in the same direction. Another important finding from the study of Swanson et al. is that the amplitude of the tubercles is important and larger amplitude bumps were found to flatten

the lift curve more than smaller bumps. The wavelength, however, does not affect the stall angle of attack (26).

The increased efficiency from adding tubercles to the leading edge of wind turbine blades is all the more significant for small-scale turbines which operate at lower Reynolds numbers. The modeling performed in this thesis delves into this theory to evaluate the effects that tubercles can have on small-scale wind energy conversion systems.

3. DESIGN OF A RESIDENTIAL-SCALE WIND TURBINE DIFFUSER USING COMPUTATIONAL FLUID DYNAMICS AND STATISTICAL ANALYSIS

While deployment of large-scale wind energy systems has continually increased in recent years, there is still little to no use of residential-scale wind energy conversion systems. This is due to their high costs and low energy output. The power output 'P' from a wind turbine is given as (28):

$$P = \frac{1}{2}\eta\rho\pi r^2 U_\infty^3 \quad (1)$$

where ρ denotes the density of wind, r is the radius of wind turbine rotor, U_∞ is the free upstream wind speed, and ŋ represents the overall efficiency of the wind turbine.

It can be noted from Equation 1 that the power of the wind turbine is directly proportional to the square of the radius and cube of the wind speed. As the size of the wind turbine and the operating wind speed are decreased, the power decreases drastically. For a low wind speed, small scale wind turbine power output is normally too low to justify its installation and operational cost. This is the main reason why residential scale wind turbines (diameter: 1m-2m (3.28-6.56 ft.) with wind speed less than 4.47 m/s (10 mph) are not commercially attractive. However, through the use of velocity enhancing components, such as diffusers, the power output can be greatly increased and thus the residential-size wind energy conversion system can be made economically viable. Diffusers are also able to allow the turbines to start at a lower speed (28), and assist in maintaining rated power output over a wider range of speeds (28). Diffusers surrounding the wind turbine blades increase the wind velocity through the turbine by creating a pressure drop at the exit of the diffuser that increases the mass flow through the system

(8). Amplifying the velocity through the turbine is important for increasing the power output because power is proportional to velocity cubed, as shown by Equation 1.

This chapter uses actuator disk theory and computational fluid dynamics (CFD) to model a variety of diffuser designs building upon the results reported in literature (7, 8, 10, 11, 28). Sorensen et al. have introduced actuator disk theory as an appropriate model for wind turbines in computational fluid dynamics (7). Ohya et al. have researched three different hollow structures to find the best configuration for a wind turbine diffuser. In their study, the models with smallest cross sections were 12 cm (4.7 in.) and the largest were 24 cm (9.4 in) (8). Ohya et al. found that a large increase in wind speed was obtained if a long diffuser body over [greater than] L/D =3 is used (8), where L is the length of the diffuser and D is the diameter of the wind turbine. Ohya et al. also found an optimal ratio of outlet area to inlet area of 2.35 in their work (8). Kishore et al. (28) used CFD to design a diffuser for a low wind speed small wind turbine of diameter 39.4 cm (15.5 in). Their study revealed that a diffuser of the length almost equal to the diameter of the turbine can augment the velocity by 1.2 times.

For the research presented in this chapter, the k-ω SST turbulence model was used based on its strengths in modeling flows that involve separation (11). Wang et al. validated the use of CFD to model the fluid flow through a turbine and showed comparative analysis between analytical and experimental results (10). A method is presented here for determining the optimal dimensions of a residential-scale wind turbine diffuser. This method involves the variation of individual parameters to understand their individual effects on the velocity amplification factor and to design the diffuser such that the power output will be a maximum. Using statistics can help the design of the

experiment to reduce the number of models and the computational time while still gathering an adequate sample set to survey the data and optimize the diffuser. The methodology is explained in section 3.1 and results are discussed in section 3.2. Section 3.3 provides details of the "optimal" diffuser based on the research conducted, section 3.4 discusses the effects of increasing inlet wind velocity on amplification factor, section 3.5 discusses the physical parameters to consider when fabricating an experimental model of this turbine and section 3.6 compares the current design with other commercially available options. Section 3.7 gives a brief summary of the diffuser optimization process and results.

3.1 Method for Optimizing the Diffuser

This chapter describes a method for optimizing a residential-scale wind turbine diffuser based on the variation of individual parameters. This design was based on unpublished results from previous research. A flow diagram of the process used for this analysis is shown in Figure 3.1. The programs discussed are JMP®, a statistical software developed by the SAS Institute with capabilities for statistical data analysis. ICEM and FLUENT are ANSYS products. ICEM has been used for building and meshing geometrical models, and FLUENT has been used to determine the flow physics of air flowing through the diffuser augmented wind turbine model.

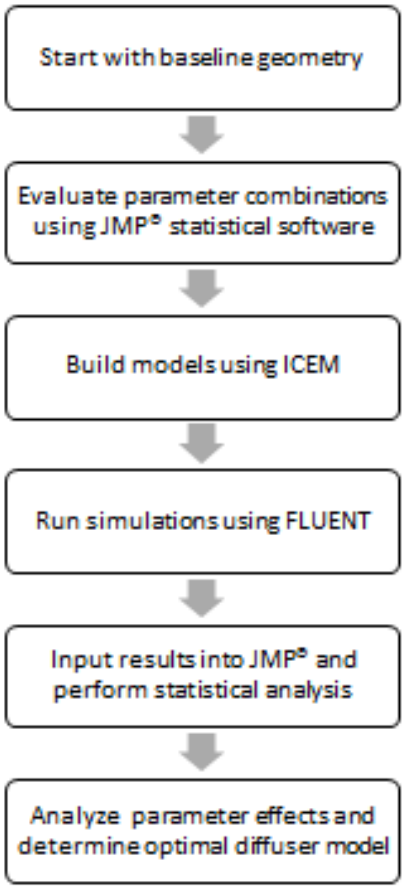

Figure 3.1. Flow diagram for the DAWT modeling

The constant parameters for the diffuser are: 1 m (3.28 ft.) diameter wind turbine rotor and a 0.25 m (0.82 ft.) flange at the outlet of the diffuser. All other geometric parameters were varied as will be discussed throughout this chapter. JMP® software was used to determine which model variations to simulate. The JMP® Custom Designer feature uses a "cooperative exchange" process to test every level of given parameter and decide whether using that level will add valuable information to the experiment design. The "cooperative exchange" process is repeated beginning at a different random point until it outputs a design that will best describe the system to be analyzed (44).

Models were built and meshed using ICEM CFD, a mesh generation software and product of ANSYS. Then the models were evaluated using FLUENT, an ANSYS CFD solver. The k-ω SST turbulence model was used in FLUENT with velocity inlet and pressure outlet boundary conditions for the fluid flow analysis. The k-ω SST model is best at predicting complex flows involving separation (11). Turbulent y^+ values along the diffuser were used to check the adequacy of the mesh size. For the k-ω SST turbulence model the y+ values should be ≤ 1; this criteria was met throughout the entirety of the DAWT modeling.

The velocity amplification factor (area weighted average wind velocity at the throat of the diffuser over free stream wind velocity) was recorded for each model calculation. Then the data was imported into JMP®, where it was analyzed to find the optimal geometries based on each method. Figure 3.2 shows one FLUENT model of a wind turbine diffuser with each parameter used in the method shown. Figure 3.3 shows the boundary conditions used in FLUENT. Table 3.1 shows the mesh variations examined during the grid refinement study.

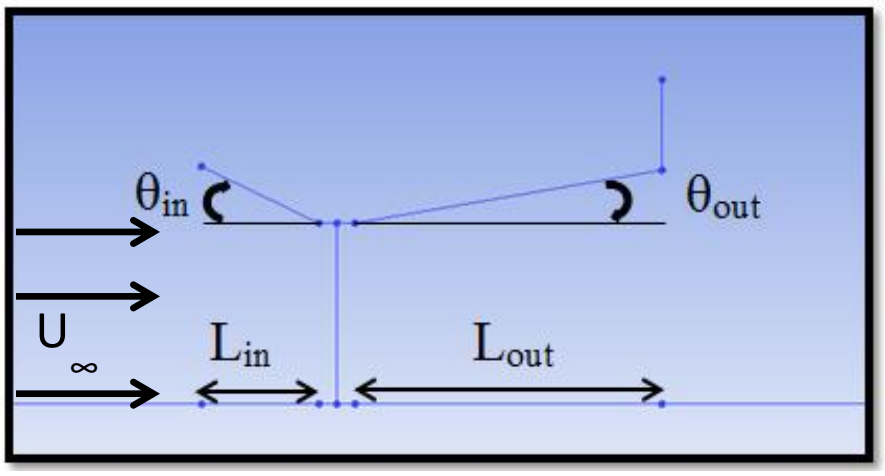

Figure 3.2 CFD model of wind turbine diffuser with each parameter shown

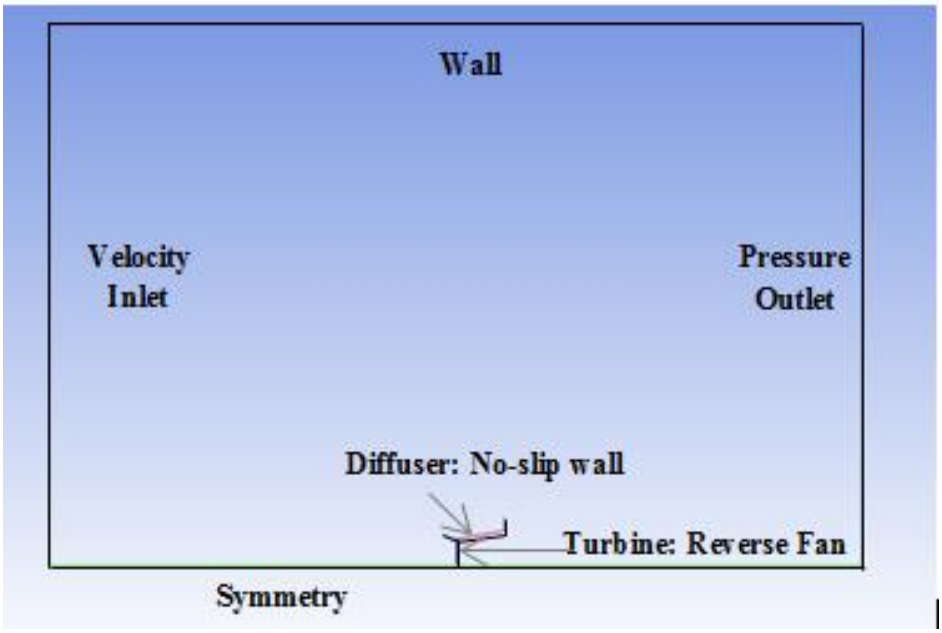

Figure 3.3 Boundary conditions for model calculation in FLUENT

Table 3.1 Grid Refinement Study for DAWT Simulation

Number of Nodes	Turbine Velocity	Percent Difference from Used Value	y+ value
105304	4.37	33%	3.95
294145	6.57	USED	0.88
555963	6.37	3%	0.77

Four different parameters were varied in this method of optimizing the wind turbine diffuser geometry. The parameters are inlet length, L_{in}, and inlet angle, θ_{in}, outlet length, L_{out}, and outlet angle θ_{out}. As shown in Figure 3.2, L_{in}, θ_{in}, L_{out}, and θ_{out} were all changed individually to measure the effects of their changes. Four different inlet lengths between 0.1 m and 0.65 m (0.33-2.1ft) were examined. The inlet angles that were evaluated were 10° through 50° in increments of 10˚. Five outlet lengths between 0.425 m and 2.125 m (1.4 -7 ft.) were inspected, and seven outlet angles between 0° and 20° were simulated. These lengths and angles were chosen based on the previous studies and taking the size of the device into account. While large outlet angles lead to flow

separation, they were simulated to examine where separation occurs and test the limits of a diffuser with a flange built for a one meter diameter wind turbine rotor.

JMP® was used to determine which combinations of the four parameters to simulate. The goal in this effort was to examine a large sample as an example and to better understand the effects of varying each parameter, but JMP®, is capable of reducing the number of samples by choosing the best models that will create a survey of the data that will provide the most informative statistical analysis. This can reduce the computational cost during research. The original way (without JMP®) would be to vary one parameter at a time and note the effects of each change. This requires more models than using JMP® (or other statistical software). The use of statistical software allows for methodical variation of parameters simultaneously because it analyzes the data while accounting for interactions between the parameters.

The models that were suggested by JMP® were randomized before analyzing the fluid dynamics of the diffusers by using FLUENT. The models that were simulated in addition to their velocity amplification factors and a designation of their level of detachment for one of the two replications are shown in Appendix A. The detachment designation follows the model of Simpson (13), in which there were four designations:

- ID: Incipient detachment, "occurs with instantaneous backflow 1% of the time"
- ITD: Intermittent transitory detachment, "occurs with instantaneous backflow 20% of the time"
- TD: transitory detachment, "occurs with instantaneous backflow 50% of the time"
- D: detachment, and this is visible because when the flow is completely detached, the velocity shows as zero or negative near the diffuser wall

These terms were designated to each model based on the visual inspection and estimation of the velocity contour plots in FLUENT. The last designation is that the flow does not separate, and this is also shown in Appendix A. The velocity amplification factor was recorded after modeling 178 different geometries in FLUENT. Results from each model that did not induce flow separation were input into JMP® statistical software to find the optimal geometry and identify significant relationships between the parameters. The statistical analysis used two replications of the data from the different geometries. The results of this analysis will be discussed in section 3.2.

3.2 Results of the Diffuser Optimization Process

The JMP® analysis for the optimization of the wind turbine diffuser showed that all parameters in the model had a significant effect on the velocity amplification factor considering all four parameters were present in the model. So, one can continue analyzing the effect of each geometric parameter on the fluid characteristics through the wind turbine diffuser. The effects of varying each parameter are shown in Figure 3.4. The different points at each level of the parameters are due to the fact that while the x-value on the graph stays the same, it has been combined with various levels of the three other parameters. For example, the L_{in} graph, graph (a) of Figure 3.4, shows multiple data points at each of the lengths analyzed because even though that length was the same, it was combined with different levels of the other parameters. For example, in one instance, the combination of parameters is L_{in} = 0.1 m, $\theta_{in} = 30^{\circ}$, L_{out} = 0.85 m, and $\theta_{out} = 0^{\circ}$ and in the next instance, the combination is L_{in} = 0.1 m, $\theta_{in} = 20^{\circ}$, L_{out} = 2.125 m, and $\theta_{out} = 4^{\circ}$.

The interactions between parameters result in different data points for the same inlet length. This is true for each parameter.

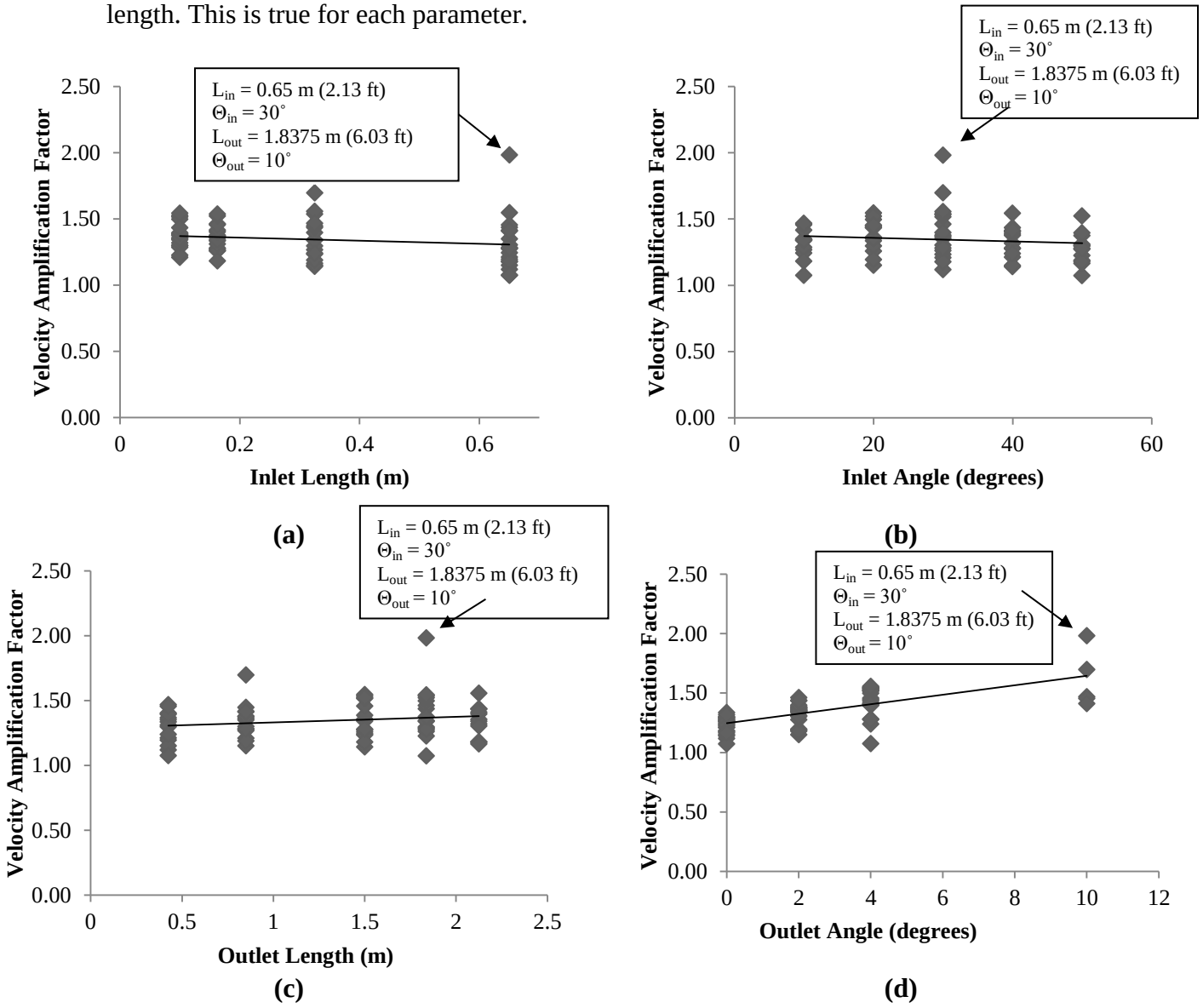

Figure 3.4 Effects of varying each diffuser parameter on the velocity amplification factor. (a) The velocity amplification factor decreases with increasing inlet length, (b) The velocity amplification factor is highest when the inlet angle is between 20˚ and 30˚, (c) As the outlet length increases, so does the velocity amplification factor, (d) as outlet angle increases, velocity amplification increases until flow separation occurs.

Using the JMP® software, the interactions between the parameters can be evaluated. For example, interaction occurs between outlet length and outlet angle, that is, when either one changes, the optimal value for the other parameter will be affected. After calculating the fluid characteristics of all of the models, it was found that flow separation

occurs for most outlet angles greater than 10˚. Eleven of the 52 diffuser models that had a 10˚ outlet angle did not experience separated flow. Of those 11 models, nine had inlet lengths of 0.325 m (1.07 ft) or more. This shows that a longer inlet length can delay the separation in the diffuser. One of the benefits of varying the parameters individually is the ability to pinpoint which parameters contribute to flow separation.

The range for the ratio of the diffuser's outlet area to its inlet area was found to compare with the work of Ohya et al. (8). They found that the optimal outlet area to inlet area ratio is 2.35 for their small-scale wind turbine. In this study, the optimal range for the ratio of outlet area to inlet area was 2.39 to 2.64. This is higher than Ohya et al. because they only tested diffuser angles up to 4˚, and the 11 out of 52 diffuser models simulated with 10˚ angles did not experience separated flow contribute to the higher outlet angle, and subsequently to the higher outlet area found in this study.

The JMP® statistical software has a "desirability" rating that determines, on a scale from 0 to 1, the desirability of the combination of selected parameters. JMP®'s desirability rating is based on piecewise functions that fit the control points of the data (29). In this analysis, JMP® was programmed to determine the desirability based on maximizing the velocity amplification factor. Velocity was used as a block in this statistical study. Table 3.2 shows the area ratio version of the diffuser parameters at the JMP® calculated "maximum desirability." The 95% Confidence Interval shows that interval within which JMP® predicts the velocity amplification factor will fall.

Table 3.2 shows the area ratios involved in the diffuser parameters with "maximum desirability." These parameters are shown in Figure 3.5.

Table 3.2 Diffuser Parameters at Maximum Desirability

Inlet Wind Velocity (m/s)	Inlet Area to Turbine Area Ratio	Outlet Area to Turbine Area Ratio	Outlet to Inlet Area Ratio	Predicted Velocity Amplification Factor	Desirability	95% Confidence Interval
1.34 (3mph)	1.26	3.01	2.39	1.68	83%	[1.46, 1.89]
2.24 (5mph)	1.20	3.01	2.50	1.88	100%	[1.73,2.03]
3.58 (8mph)	1.2	3.01	2.5	1.94	82%	[1.79, 2.08]
4.47 (10 mph)	1.14	3.01	2.64	1.90	100%	[1.76, 2.04]

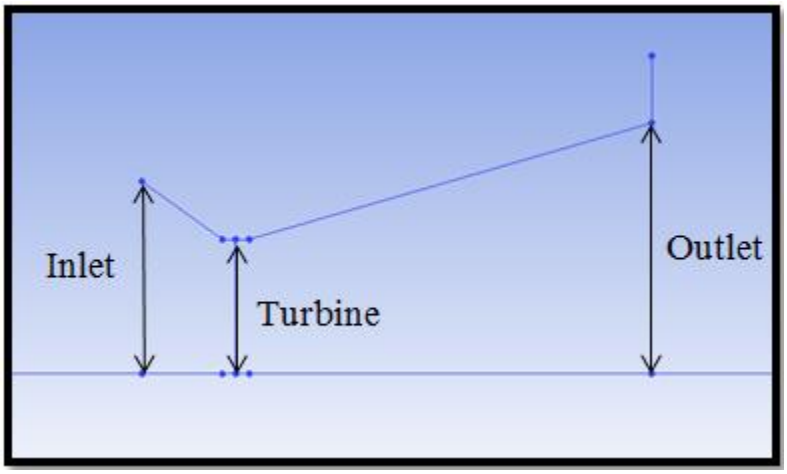

Figure 3.5 CFD model with elements of the area ratios shown

Of the combinations of parameters simulated, the models with the "maximum desirability" are shown again in Table 3.3 with their individual parameters. All models throughout this research have a turbine rotor area of 0.785 m^2 (8.5 ft^2). The "maximum desirability" models shown in Table 3.3 have a maximum diffuser area of 2.362 m^2 (25.42 ft^2).

Table 3.3 Individual Diffuser Parameters for Maximum Desirability

Inlet Wind Velocity (m/s)	Inlet Length (m)	Inlet Angle	Outlet Length (m)	Outlet Angle	Predicted Amplification Factor
1.34 (3 mph)	0.1 (0.33 ft.)	40	2.125 (7 ft.)	10	1.68
2.24 (5 mph)	0.1 (0.33 ft.)	30	2.125 (7 ft.)	10	1.88
3.58 (8 mph)	0.1 (0.33 ft.)	30	2.125 (7 ft.)	10	1.94
4.47 (10 mph)	0.1 (0.33 ft.)	20	2.125 (7 ft.)	10	1.90

Another point to note is the increase in predicted amplification factor with an increase in inlet wind velocity. Attention to that phenomenon is found in section 3.4. To determine whether the diffuser is an efficient way to increase the power output of the wind turbine, the power output was compared as the ratio between the diffuser augmented wind turbine (DAWT) and a bare wind turbine of the same rotor area (P_o/P), and the ratio of the power output of a turbine with the area of the outlet area of the diffuser (largest cross-sectional area of diffuser) and the power output of the bare turbine (P_1/P). Figure 3.6 gives a pictorial reference that shows where each of these variables to calculate power is measured.

If the values for each power calculation are substituted into Equation 2 the ratios become

$$\frac{P_o}{P} = \frac{U_o^3}{U_\infty^3} \tag{2}$$

for the DAWT versus the bare turbine of the same size rotor. The variable U_o is the wind velocity at the turbine blades. The second equation is for the power output if the turbine was created with the outlet area of the diffuser versus the bare turbine:

$$\frac{P_1}{P} = \frac{A_1}{A_o} \tag{3}$$

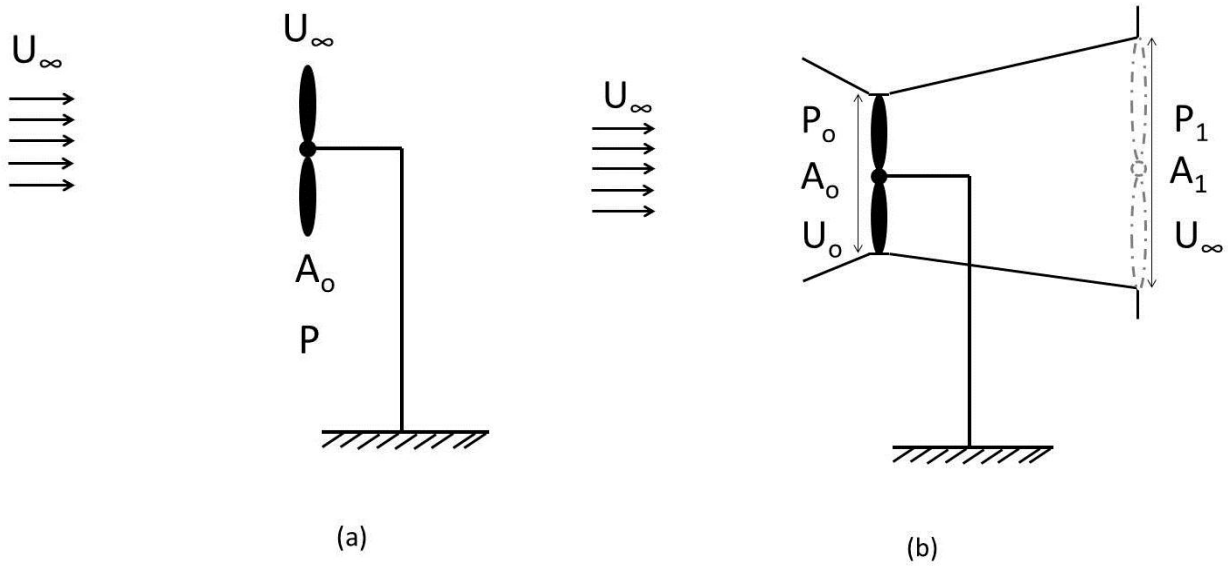

Figure 3.6. Variables used to calculate the power of a bare turbine (a) versus those used to calculate the power of a diffuser augmented wind turbine (P_o) and a wind turbine with the largest diameter of the diffuser as the diameter of the rotor (P_1) (b).

In order to understand whether a diffuser to amplify the power output of the turbine is even useful, it is worth considering these ratios of the power. The second important ratio involves the largest diameter of the wind turbine diffuser. If the area of a rotor of the largest diameter were used, would it be more powerful than a smaller wind turbine rotor augmented with a diffuser? This is an important question to answer when deciding whether or not to use a diffuser. Figure 3.7 shows each of the power ratios plotted against velocity amplification factor. It is expected that all the power ratios will increase as velocity amplification factor increases.

When considering the largest area of the diffuser as the area for the power calculation, it is shown that the power ratio still increases with velocity amplification factor, but depending on the geometry of the duct (the magnitude of the largest diameter) it is usually less than P_o/P, which infers that the diffuser still increases the power output more than a bare turbine with the dimensions of the largest area of the diffuser.

When designing a wind energy conversion system, one always needs to ensure that a wind turbine diffuser will result in a higher power output than the equivalent diameter bare turbine. The overall requirements and constraints of the turbine application should be considered when evaluating the utility of the diffuser.

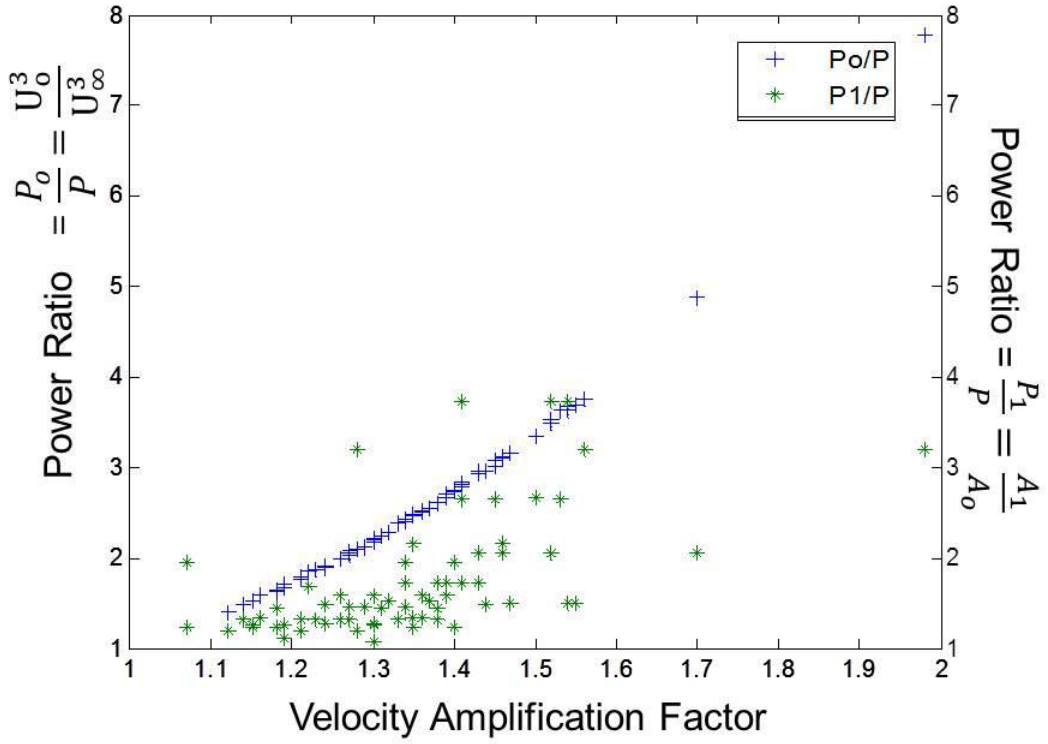

Figure 3.7 Power ratios versus velocity amplification factor. The ratio of the DAWT power to the bare turbine power (P_o/P) increases consistently with velocity amplification factor. The ratio of the power for the largest diameter of the diffuser to the power of the original turbine (P_1/P) is greater or less than (P_o/P) depending on the geometry.

3.3 Diffuser Refinement Based on Results from Statistical Diffuser Optimization

Based on the information obtained from the diffuser optimization process using variation of individual parameters, it is clear that moderately-angled inlet (0.1 m (0.33 ft) and 20˚-30˚) coupled with a long outlet with the highest angle that does not cause flow

separation (in this case 1.5 m (4.9 ft) and 5˚) will result in the greatest velocity (and therefore power) amplification. Utilizing this information, more diffuser models were designed and simulated using ANSYS FLUENT. Since all solutions for models calculated with a 4˚ outlet angle did not result in flow separation, and some of the models with 10˚ outlet angles did not result in flow separation, the parameters in Table 3.4 were examined to see which would be the "optimal" diffuser parameters.

Table 3.4 Refined Diffuser Parameters and Results

L_{in} (m)	θ_{in} (˚)	L_{out} (m)	θ_{out} (˚)	Velocity Amplification Factor	Flow Features
0.1	15	1.5	5	1.53	Detached
0.1	20	1.5	5	1.55	Not Separated
0.1	25	1.5	5	1.56	Not Separated
0.1	15	1.5	7	1.50	Detached
0.1	20	1.5	7	1.56	Detached
0.1	25	1.5	7	1.65	Not Separated
0.1	15	1.5	9	1.47	Detached
0.1	20	1.5	9	1.56	Detached
0.1	25	1.5	9	1.61	Detached

For angles greater than 5˚, the flow tends to separate. The higher inlet angles (θ_{in}) postpone separation in the diffuser (as long as they are not so large that the flow separates at the inlet). After examining the results from simulating these models in FLUENT, the optimal diffuser design for a wind turbine with a one meter diameter rotor is an L_{in} of 0.1 m (0.33 ft.), and θ_{in} of 20˚, an L_{out} of 1.5 m (4.9 ft.), and a θ_{out} of 5˚. These parameters were chosen because it is best to have a short, moderately angled inlet, and the higher angled outlet section. Since structural issues can occur if the diffuser is too long, the outlet length is limited to 1.5 m, or $L_{out}/D = 1.5$, where D is the diameter of the turbine rotor. FLUENT simulated velocity contour plots of each of the "refined" models are shown in Figure 3.8.

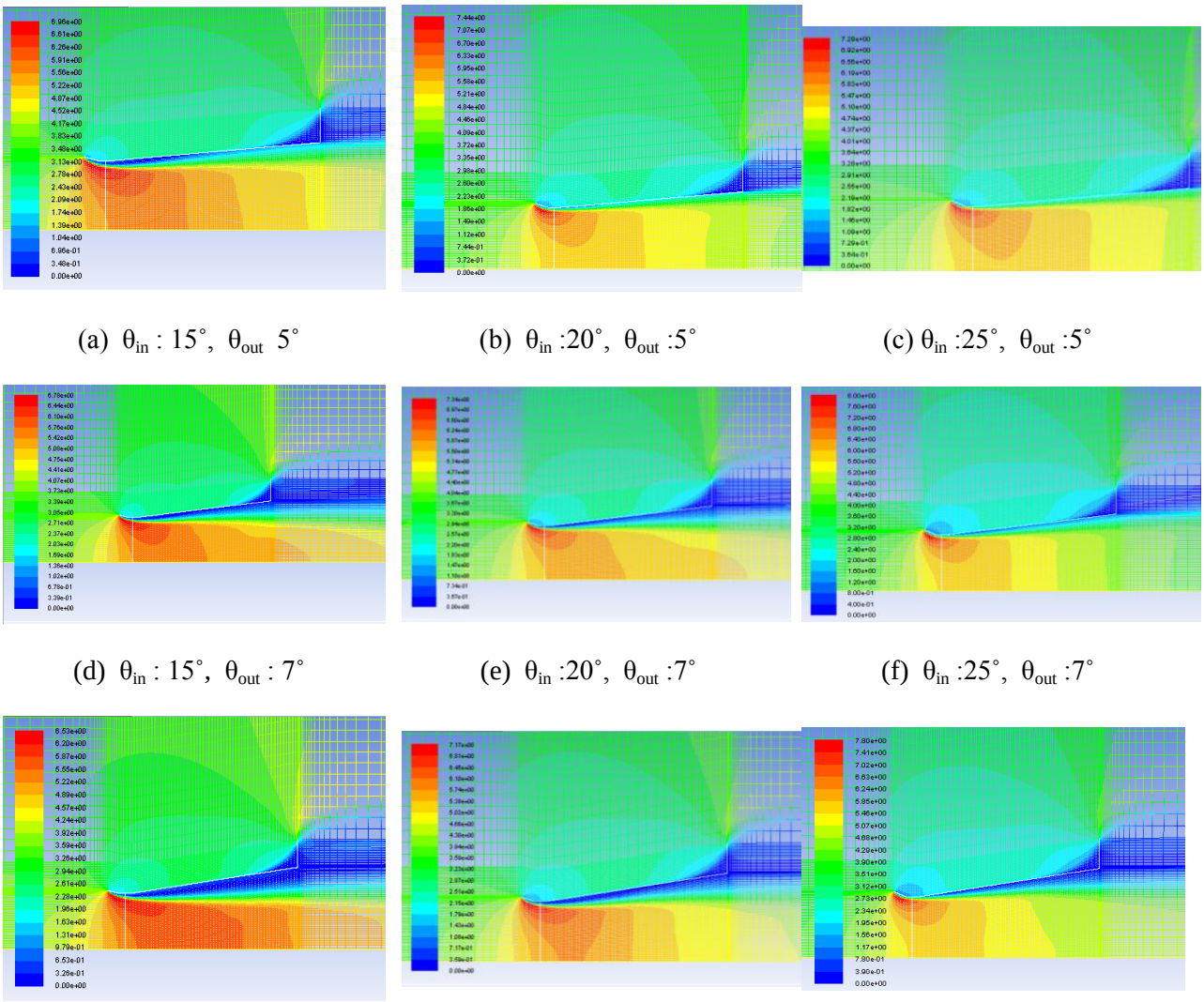

(a) θ_{in} : 15˚, θ_{out} 5˚ (b) θ_{in} :20˚, θ_{out} :5˚ (c) θ_{in} :25˚, θ_{out} :5˚

(d) θ_{in} : 15˚, θ_{out} : 7˚ (e) θ_{in} :20˚, θ_{out} :7˚ (f) θ_{in} :25˚, θ_{out} :7˚

(g) θ_{in} : 15˚, θ_{out} : 9˚ (h) θ_{in} :20˚, θ_{out} :9˚ (i) θ_{in} :25˚, θ_{out} :9˚

Figure 3.8. FLUENT simulations of the refined diffuser models. Each model has an inlet length of 0.1 m and an outlet length of 1.5 m. The inlet and outlet angles are given next to their symbols.

Figure 3.8 demonstrates how the flow remains attached for longer x/L (where x is the location on the diffuser) when the inlet angle is larger. The blue sections show a region with flow separation. The unsteady conditions caused by flow separation can be detrimental to the turbine and will cause it to function improperly. In Figure 3.8 it is also visible that separation begins to occur at 7˚ outlet angles and becomes more severe as the outlet angle is increased to 9˚. The velocity amplification factor was 1.55 for both a 20˚

and 25˚ inlet angle coupled with a 0.1 m (0.33 ft.) inlet length, 1.5 m (4.9 ft.) outlet length, and 5˚ outlet angle. For this reason, the geometry with L_{in} = 0.1 m, θ_{in} = 20˚, L_{out} = 1.5 m, and θ_{out} = 5˚ was chosen as optimal for the diffuser. The outlet to inlet area ratio for this model is 1.4.

Table 3.5 shows the velocity amplification factor, and the potential power output (Equation 1 with 0.2 as η) for the refined model as evaluation parameters. Each evaluation parameter remains relatively constant through varying inlet wind velocities. The velocity amplification factor of 1.55 is equal to a power amplification of 3.73 because power is proportional to velocity cubed.

Table 3.5 Refined Diffuser Evaluation Parameters

Inlet Wind Velocity (m/s)	Velocity Amplification Factor	Power Output (W)
1.34 (3 mph)	1.54	0.85
2.24 (5 mph)	1.55	4.05
3.58 (8 mph)	1.55	16.44
4.47 (10 mph)	1.55	32.25
5 (11.2 mph)	1.56	45.35

Using this refined model and two other models examined previously, a short study was performed to determine the effect of increasing inlet wind velocity on the amplification factor. Results are discussed in section 3.4.

3.4 Effects of Increasing Inlet Wind Velocity on Amplification Factor

During the analysis of the newly optimized diffuser model, a small (2% total) increase in velocity amplification factor was observed as the inlet wind velocity increased. To analyze this further, two more diffuser geometries were simulated and their velocity amplification factors were recorded when the wind speed was 1.34 m/s (3 mph), 3.58 m/s (8 mph), 4.47 m/s (10 mph), 6.71 m/s (15 mph), and 8.94 m/s (20 mph). Inlet wind speeds greater than this are uncommon for small-scale wind applications at altitudes less than 30 m (98.4 ft). The dimensions of the models examined are given in Table 3.6 and the velocities at the turbine along with the velocity amplification factor are given in Table 3.7. The results are plotted in Figure 3.9.

Table 3.6 Diffuser Dimensions for Inlet Wind Velocity Increase

Model	Inlet Length (m)	Inlet Angle (°)	Outlet Length (m)	Outlet Angle (°)
1	0.1	20	1.5	5
2	0.1625	20	1.5	2
3	0.1	30	1.5	4

Table 3.7 Velocities Amplified by the Various Wind Turbine Diffuser Models

	Model 1		Model 2		Model 3	
Inlet Wind Velocity (m/s)	Turbine Wind Velocity (m/s)	Velocity Amplification Factor	Turbine Wind Velocity (m/s)	Velocity Amplification Factor	Turbine Wind Velocity (m/s)	Velocity Amplification Factor
1.34	2.07	1.54	1.82	1.36	2.06	1.54
3.58	5.56	1.55	5.20	1.45	5.52	1.54
4.47	6.95	1.55	6.50	1.45	6.78	1.52
6.71	10.64	1.59	9.78	1.46	10.37	1.55
8.94	14.18	1.59	13.05	1.46	13.84	1.55

According to the calculations, the velocity will be amplified even more as the inlet wind velocity is increased. While only inlet wind velocities feasible for small-scale applications are reviewed, this work could be extended to examine where the amplification factor levels off. This would give an amplification limit for the diffuser being modeled. Wind tunnel and field testing could be used to verify the fluid dynamics involved in this phenomenon.

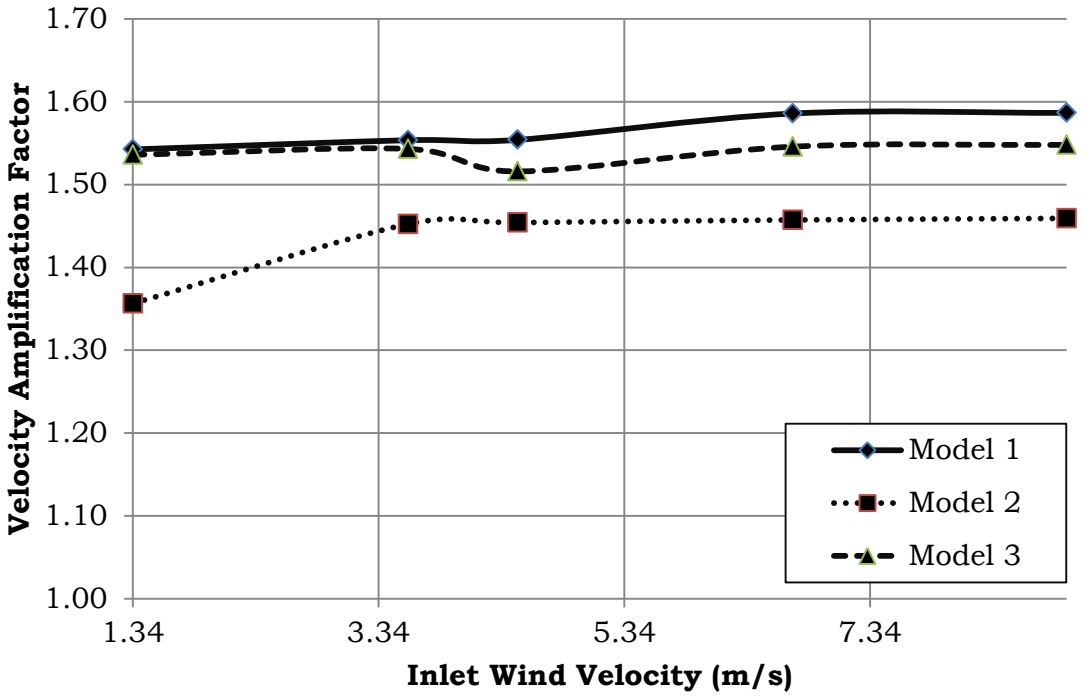

Figure 3.9. Velocity amplification factor as a function of inlet wind speed. As the inlet wind speed increases, there is a small increase in velocity amplification factor.

3.5 Physical Considerations for the Refined Diffuser Model

While the computational model in this chapter compares reasonably well to other models both experimental and computational information found in literature, (8, 28), there are some physical considerations that could improve its flow characteristics.

Physical considerations include the shape of the transitions from the inlet to the conical area where the turbine is located to the diffuser outlet and the revolutions per minute (RPM) at which the blades within the diffuser are spinning. The model shown in Figure 3.2 was simple to create and discuss. However, the sharp edges should be more rounded when the physical model is created and tested experimentally. This will guide the air flow more smoothly through the diffuser and improve the pressure distribution slightly. This is because minor losses may be larger when there are sharp edges than when the flow is gradual and sharp angles are avoided (45).

In order to reduce the effects of separation, the pressure distribution within the diffuser should be considered in the design. The pressure recovery coefficient, C_{pres}, measures the ratio of static pressure rise across the diffuser to the inlet dynamic pressure (45); given as:

$$C_{pres} = \frac{p_2 - p_1}{{}^1/_2 \rho U_\infty^2} \quad (4)$$

where p_2 is the pressure of the fluid entering the diffuser, and p_1 is the pressure as the fluid leaves. The variable ρ represents the air density (1.225 kg/m^3) and U_∞ is the inlet wind velocity in m/s. The pressure distribution along the refined diffuser model discussed in section 3.4 is shown in Figure 3.10. Negative x values represent the inlet of the diffuser, the locations between x = (-0.05, 0.05) are the conical section of the diffuser where the turbine blades are located. The positive x values are the diffuser outlet.

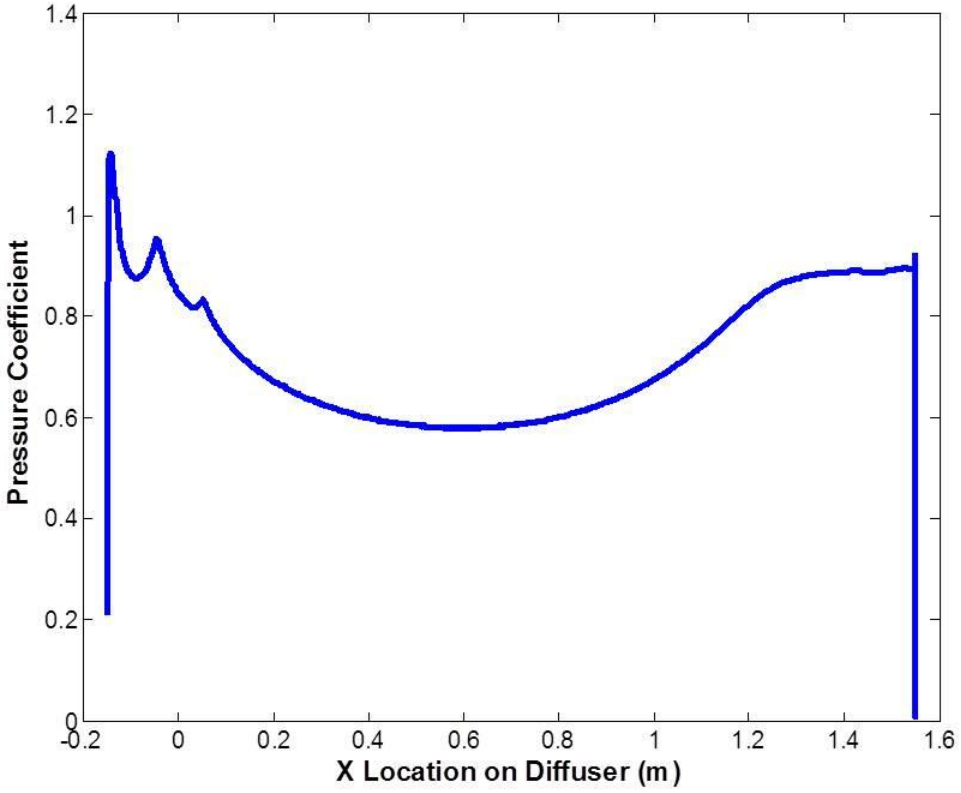

Figure 3.10 Pressure coefficient along the diffuser wall. The vertical lines represent the ends of the diffuser and are not representative of the actual pressure just outside of the diffuser. This graph shows solely the distribution along the diffuser wall.

As seen in Figure 3.10, the lowest pressure recovery coefficient, C_{pres} = 0.58, exists at the location 0.6 m, which corresponds to about 37% of the diffuser outlet length when measuring from left to right beginning at the end of the turbine area. Visible in Figure 3.8 b, is the fact that this 37% location is critical for the flow to remain attached as it does. This is shown by the small blue area that suggests the ability for the flow to detach, but failure to do so due to the placement of the low-pressure point, the flow is able to overcome the pressure gradient and remain attached to the diffuser wall. This continuous attachment is critical for the performance of the diffuser.

Another item that is extremely important but was not explicitly modeled here is the actual rotor. As discussed in section 3.2, this was modeled as a “reverse fan” boundary condition. It is assumed that the turbine has three blades, and a tip speed ratio of 3.5 as does the turbine tested in Chapter 5 with a straight edge. At the wind speeds simulated (1.34-4.47 m/s (3-10 mph)) the resulting revolutions per minute (RPMs) are shown in Table 3.8. The RPMs at 8.94 m/s (20 mph) are also shown for reference to other turbines and their high rated wind speeds. To compare to the turbine discussed in the next section, 3.6, the RPM values were also calculated for the Renewable Devices “Swift” turbine’s rated wind velocity of 12 m/s.

Table 3.8 RPM When the Tip Speed Ratio is 3.5

Incoming Wind Velocity (m/s)	Amplification Factor of "Refined Diffuser"	Velocity at the Turbine (m/s)	Radial Velocity (rad/s)	RPM
1.34	1.54	2.0636	3.61	34.49
2.24	1.55	3.472	6.08	58.02
3.58	1.55	5.549	9.71	92.73
4.47	1.55	6.9285	12.12	115.78
8.94	1.56	13.9464	24.41	233.06
12	1.56	18.72	312.84	357.53

Even at the rated wind velocity of the Swift turbine, the diffuser augmented turbine design discussed in this chapter only reaches a high of 358 RPM. Thus, an appropriate gear train will need to be designed to reach the optimal RPM of the motor, which is usually between 1400-1800 RPM for the power generation capabilities of this diffuser augmented wind turbine.

3.6 Comparisons with Current Commercially Available Turbines

Two diffuser augmented wind turbines were found on the commercial market: the Swift Turbine from the Scottish company Renewable Devices (30), and the Aeropoint

from United States company Marquiss Wind Power. The Marquiss turbine is aimed at businesses for use on flat warehouse roofs and similar surfaces (31). It is 19 ft. tall and has a square duct surrounding the blades. The company advertised a two to seven year pay-back period for money spent on its purchase and installation (31). The Swift Turbine from Renewable Devices has a round diffuser ring, which only encompasses the blades, not extending past them (30). This turbine has a swept area of 3.4 m^2, and a start up speed of 3.4 m/s. Its rated power is 1.5 kW. Both devices are larger than the DAWT being developed by CEHMS. Table 3.9 compares the Swift specifications and the CEHMS turbine (there were no available specifications for the Aeropoint turbine). The rated power for the Swift turbine is based on a rated wind speed of 12 m/s, so this wind speed was also used to calculate the CEHMS turbine's rated power.

Table 3.9 CEHMS DAWT Compared to Commercial DAWT

	Renewable Devices "Swift" (30)	CEHMS	Scaled Up CEHMS
Rotor Radius (m)	1	0.5	1
Diffuser's Largest Radius (m)	1.04	0.63	1.26
Swept Area (m^2)	3.4	0.785	3.14
Rated Power (W)	1500	631	2475

Since the CEHMS turbine has less than a third of the area of the "Swift," and power is proportional to the area, if we scaled up the CEHMS turbine and all other parameters remained constant, it could produce 2475 W, which is greater than the Swift turbine. However, an efficiency of η=0.2 is used in the power calculation for the CEHMS turbine ($P = \frac{1}{2}\rho\eta AV^3$), and Renewable Devices may have calculated the Swift turbine's

power differently. Additionally, the CEHMS turbine requires further testing as all current results thus far are theoretical.

3.7 Conclusions and Recommended Future Work on the Diffuser Augmented Wind Turbine

The ability of residential scale wind turbines to provide significant magnitude of energy depends on their ability to increase the velocity of the wind flowing through the turbines' blades. To this point, well-designed diffusers are important to understand and implement. Statistics can be used to determine the appropriate wind turbine diffuser parameters to model and also to determine which interactions between parameters are significant. The use of statistics can allow researchers to test a smaller number of models than if they were to vary parameters individually. This reduces the computational cost of optimization. The methods described in this chapter can be used to determine optimal geometries for such a diffuser.

The optimal diffuser geometry for a one-meter, residential-scale wind turbine was found to be a 0.1 m (0.33 ft.) inlet with a 20˚ inlet angle, and a 1.5 m (4.9 ft.) outlet section with a 5˚ angle. This combination results in a velocity amplification factor of 1.55 which translates to a power amplification factor of 3.73. While these specific parameters are important for this design, it is important to consider the limitations of each design situation.

The velocity amplification factor was also found to increase as the inlet wind velocity increases. This is an interesting phenomenon that requires further examination. Physical considerations were discussed in section 3.5 and the refined diffuser model was

compared to commercially available turbines on the market in section 3.6. Recommended future work includes wind tunnel testing of a scale model of the refined diffuser geometry to validate the computational results.

4 TWO-DIMENSIONAL CFD MODELING OF A VERTICAL AXIS WIND TURBINE

Vertical axis wind turbines are naturally omni-directional, but are often overlooked wind energy conversion systems. Research on VAWTs has increased recently due to new developments regarding their ability to increase efficiency by an order of magnitude in a wind farm setting (4), and the renewed interest in smaller scale wind energy conversion systems. Horizontal axis wind turbines are historically more efficient and more suited to large-scale applications, but vertical axis wind turbines are capable of starting at much lower wind speeds (1.5 m/s (3.36 mph) vs. 4.5 m/s (10.07 mph) for a 1 m (3.28 ft) turbine diameter) (32). This ability makes them attractive options for small-scale wind energy conversion systems which operate at lower altitudes at lower wind speeds. Lower operation speeds also make VAWTs less dangerous for wildlife (20).

This chapter describes power coefficient for a small-scale VAWT that uses a NACA 0018 airfoil for the straight blades extruded from aluminum. Six-blades will allow the turbine to spin and generate electricity with desired structural rigidity. The concept was for this turbine to be useful both in a single turbine setting and in a potential wind farm.

4.1 System Description of the Vertical Axis Wind Turbine Prototype

The design for the vertical axis wind turbine consists of six blades spaced 60˚ apart upon a six meter high vertical post. The blades are connected at the top and bottom, and are extruded from aluminum NACA 0018 airfoils. Each blade consists of an airfoil of 87.32 mm (3.44 in) chord length, extruded to be an elliptical arc 937.09 mm (36.89 in)

from the center. The vertical length of the turbine is 3.2 m (10.5 ft). This geometry was designed by Jesper Thomsen (33) and is shown in Figure 4.1.

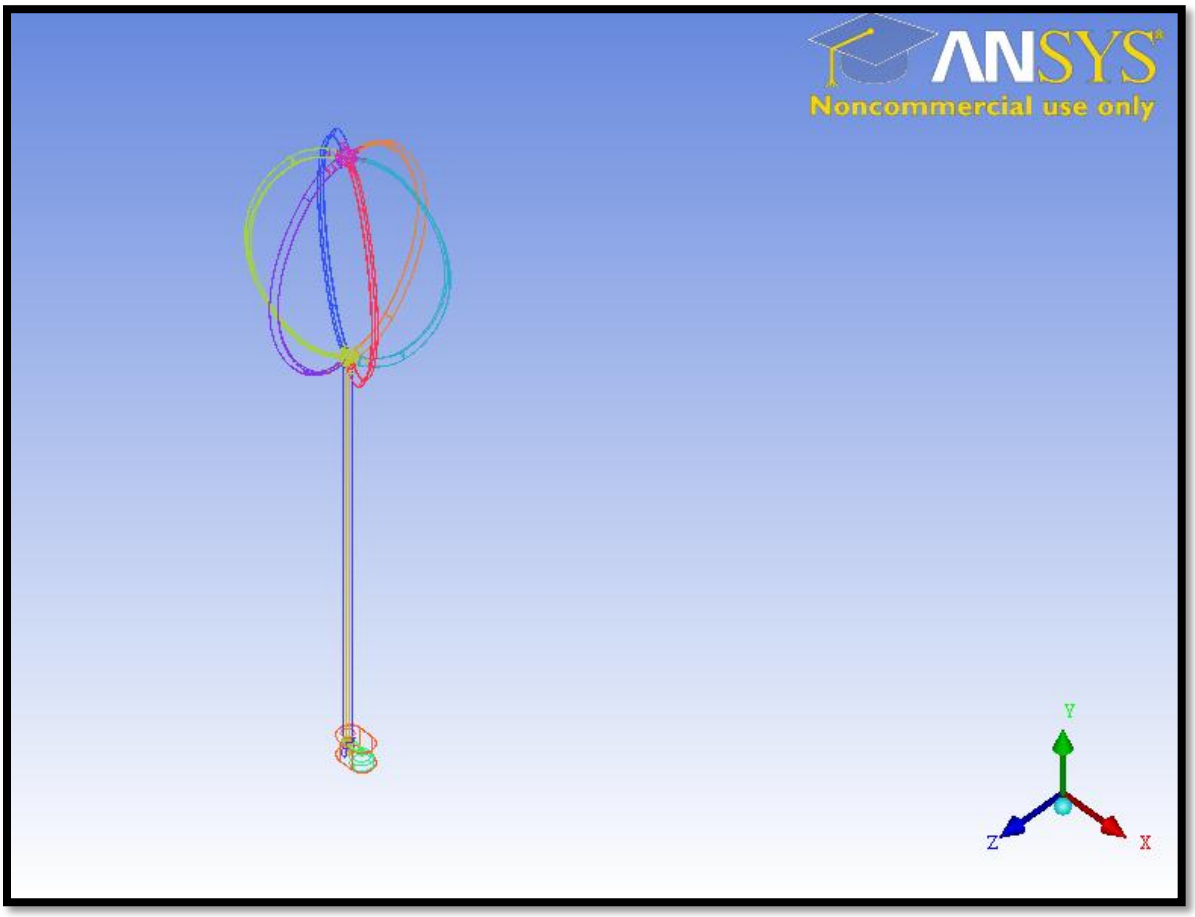

Figure 4.1 CAD drawing of the VAWT design. The mounting pole is six meters high, the profile of each blade is 87.32 mm (3.44 in), the radius of the turbine is 937.09 mm (36.89 in), and the length of each blade is 3200 mm (10.5 ft). *Note: This drawing was created by Jesper Thomsen (33) and is used in this thesis with his permission.

The airfoil aspect ratio (H/C where H is the height of the airfoil and C is the chord length) was 2.81 and the chord ratio (C/R where R is the turbine radius) was 0.093. The tip speed ratio measures how fast the blades tips are spinning relative to the incoming wind. The tip speed is the speed seen by the tip of the turbine blade, and is equal to $R\omega$ where ω is the angular velocity of the wind turbine. Thus, the tip speed ratio is the ratio

of the speed at the blade tips to the wind speed and can be calculated as such when both speed values are known.

4.2 Validation of a Single Airfoil

Before modeling the whole six-bladed VAWT, a study using a single airfoil was performed to validate the FLUENT modeling technique. This task is complex due to the inadequacy of many turbulence models to capture accurate flow characteristics over an airfoil at low Reynolds numbers. The airfoil was simulated at a chord Reynolds number of 40,000 and was calculated using the average wind speeds in Denmark since the turbine design originated in that country. After running simulations at various angles of attack (α), the values for lift and drag coefficients were compared with accepted tabulated data from Sheldahl et al. (18). The NACA 0018 airfoil was not experimentally tested during Sheldahl et al.'s research, but data for its lift and drag coefficients were extrapolated from a computer code called PROFILE and the information from the NACA 0009, NACA 0012, NACA 0015, and NACA 0012H profiles that were tested experimentally (18). This data has been used in validating many other small-scale wind efforts ((34) and (35) are a few examples).

4.2.1 Review of Modeling Low Reynolds Number Turbulence

Evaluating the Navier-Stokes equations is a difficult task for many different flow situations. At low Reynolds numbers, prior researchers have tried to implement their own methods to achieve accurate fluid flow results. Table 4.1 is a review of information available in literature for modeling airfoils approximately 0.5 m (1.64 ft) or less in chord

length for use in vertical axis wind turbines. Very few of these studies modeled the systems in realistic ranges of Reynolds numbers. This is most likely due to the issues with modeling the flow surrounding the airfoils at lower Reynolds numbers.

Table 4.1 Review of Turbulence Models Used for Low Reynolds Number Airfoil Simulation

Author	Airfoil Modeled	Chord Length (m)	Turbulence Model Used	Reynolds Numbers Tested	Inlet Wind Speeds tested
Untaroiu (20)	NACA 0018	0.083	k-epsilon with scalable turbulent wall function	Equates to ~ 32000	6 m/s
Mukinovic (36)	NACA 4418	0.5	k-omega SST	850000	equates to 26.66 m/s
			k-omega SST	850000	equates to 26.66 m/s
Olsman et. al. (37)	NACA 0018	0.165	Experimental only	10000, 100000	equates to 0.95-9.5 m/s
Hameed and Afaq (19)	NACA 0015	0.2062	Used DESFOIL	??	??
Timmer, et. al. (38)	NACA 0018	0.1-0.15	Used RFOIL and XFOIL	150000, 100000	equates to 10.45 - 23.52 m/s
Maughmer and Coder (22)	E 387, S406, S407, S411, S414, and the S415	0.152-0.533	4-equation turbulence model (Transition SST)	E387 at 300,000	equates to 8.83 - 31 m/s
				S415 at 2,000,000	equates to 58.8 - 206 m/s
Sabaeifard (39)	NACA0018 and S1210	??	k-epsilon RNG	35000 (based on blade length - would give a blade length of 0.5488 m)	10 m/s

According to Sharman (40) average wind speeds for Denmark are between 6.5 and 7.5 m/s (14.5 – 16.8 mph) and this is a country known for its high opportunities for wind power. For a chord length of 0.5 m, this equates to a Reynolds number of 240,000, but only two studies in Table 4.1 actually tested chord lengths that long. For the smallest chord in the table, 0.083 m from Untaroiu (20) the Reynolds number would be 35,000 –

40,000. Chord lengths near 0.1 m are more typical of small scale vertical axis wind turbines as evident in Table 4.1. Recall that the chord length used for the model in the present research is 0.08732 m. Regardless, Table 4.1 shows that many researchers tested their models at much higher Reynolds numbers than are reasonable for the small-scale wind applications.

4.2.2 Calculation Strategy

A grid refinement study found the optimal number of nodes for the airfoil validation to be 712,700. Calculated and experimental lift and drag coefficients from Sheldahl et al. (18) are given in Table 4.2 with their corresponding percent error for four different amounts of nodes. After 712,700 nodes the accuracy for predicting the lift coefficient does not significantly increase.

Table 4.2 Calculated vs. Experimental Lift and Drag Coefficients for Various Mesh Densities at an Angle of Attack of 5°

Number of Nodes	Calculated C_L	Experimental C_L	C_L % Error	Calculated C_D	Experimental C_D	C_D % Error
277600	0.32061	0.4117	22%	0.10598	0.0247	329%
641400	0.380817	0.4117	8%	0.047124	0.0247	91%
712700	0.478933	0.4117	16%	0.035622	0.0247	44%
1112500	0.36501	0.4117	11%	0.042331	0.0247	71%

The meshing method used for generating the mesh around the airfoil is a C-grid as shown in Figure 4.2. The boundary conditions are denoted in Figure 4.3. Rather than rotate the airfoil, the angle of attack was changed by changing the velocity components of the incoming wind.

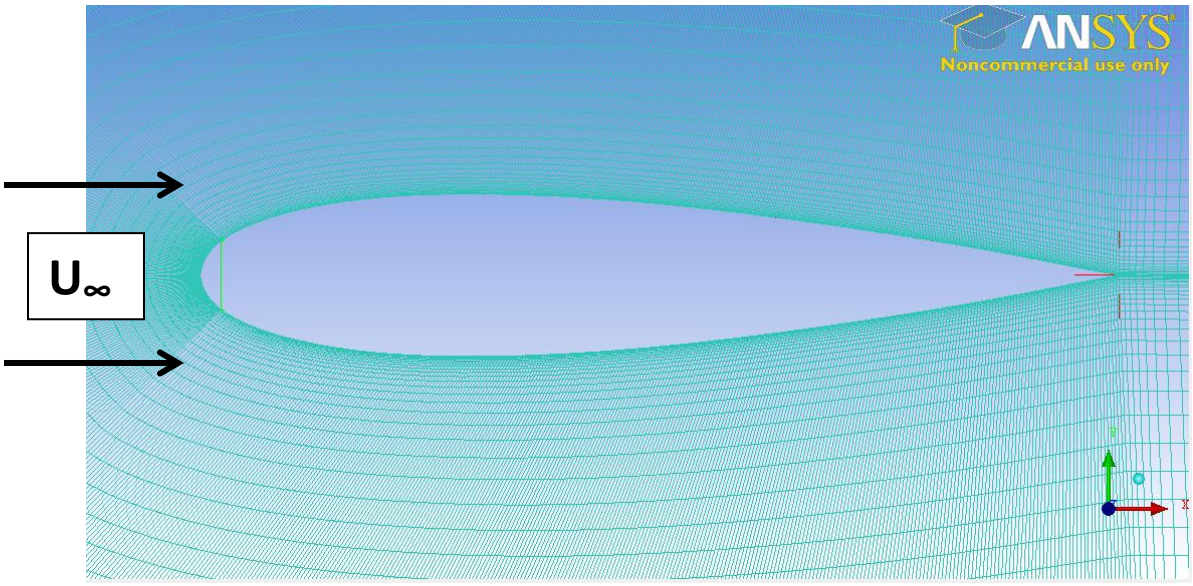

Figure 4.2 C- Grid mesh for the NACA 0018 airfoil.

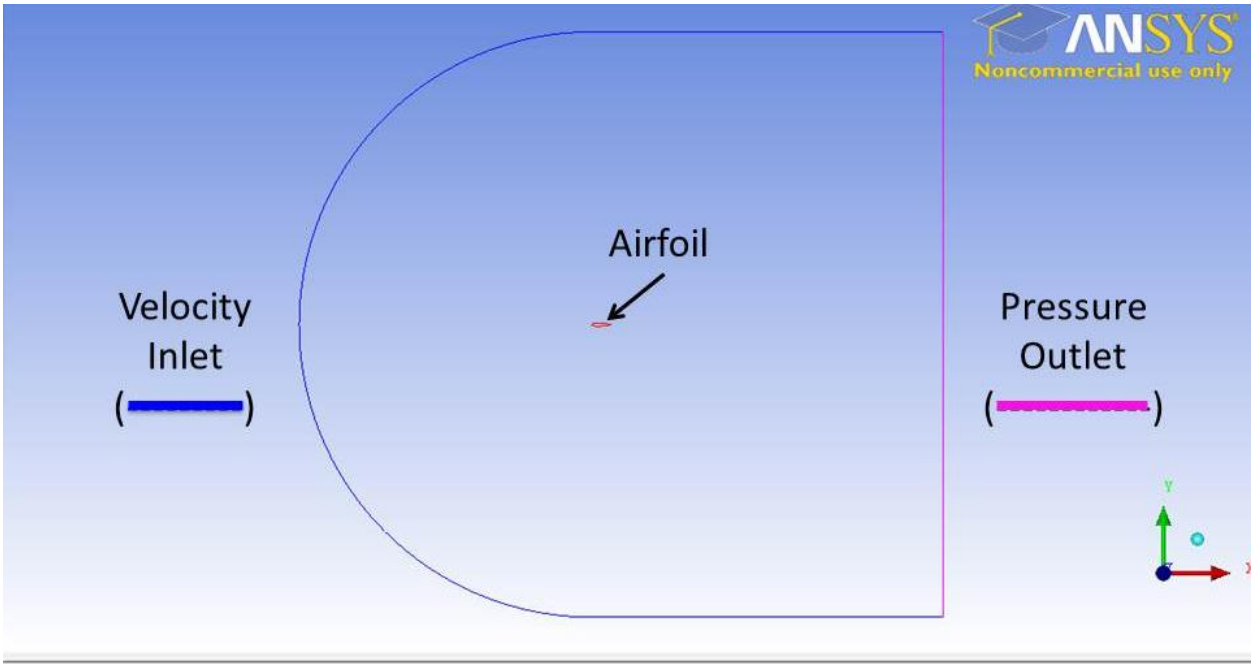

Figure 4.3. Boundary conditions for the airfoil model. The large farfield is such that the flow is fully developed and it will not be affected by the pressure outlet.

The transition SST model with curvature correction was used after trying all of the various turbulence models shown in Table 4.1. Maughmer et al. also found higher

accuracy for the results using this model in their study (22). They found that the transition SST model predicts laminar, transition, and turbulent reattachment well and the results were comparable to those of Sheldahl et al. (18).

4.2.3 Results from Airfoil Validation

After investigating all of the methods of modeling turbulence in Table 4.1 using the NACA 0018 airfoil at Re = 40,000 to verify that CFD can provide accurate results, it was found that the lift coefficient and drag coefficient were incorrect in FLUENT. The Transition SST turbulence model was the least inaccurate of all the methods attempted. Data from using the k-ε RNG model and k-ω SST model are shown in the Appendix. The k-ε RNG model approximated the drag coefficient within 6%, but the lift coefficient was off by over 70%. The k-ε RNG model has been renormalized from the original k-ε model, which is for high Reynolds number flows, to account for low Reynolds number effects (46). The k-ω SST model allows for an appropriate treatment of boundary layer effects by gradually transferring between the k-ω model and k-ε model from the inner region of the boundary layer to the outer layer respectively (46). The transition SST model was shown to balance the approximation of the lift and drag coefficients. It was also proven to be the best available model in this commercial package by Maughmer et al. (22). The benefits of the transition SST model are that it couples the k-ω SST model's transport equations with equations for intermittency and transition onset criteria (46). It has been crafted to work for low free-stream turbulence situations (46). Tables 4.3 and 4.4 show efforts using the Transition SST Model with curvature correction at a chord Reynolds

number of Re = 40,000 and Re = 360,000. Since the NACA 0018 airfoil is symmetric, only values for positive angles of attack are reported.

Table 4.3 Airfoil Characteristics when Re = 40,000

Inlet Wind Velocity = 0.6272 m/s

Angle of Attack	Drag Coefficient	Tabulated C_D	Percent Error	Lift Coefficient	Tabulated C_L	Percent Error	y+ Value
0	0.031044	0.0214	45%	0.189946	0	0.1899*	0.553363
5	0.035622	0.0247	44%	0.478933	0.4117	16%	0.901601
10	0.114785	0.062	85%	0.334246	0.2108	59%	0.574055
14	0.167714	0.158	6%	0.40037	0.0489	719%	0.622139

*This value represents the absolute error rather than the percent error since calculating the percent error would require dividing by zero in this case.

Table 4.4 Airfoil Characteristics when Re = 360,000

Inlet Wind Velocity = 5.64 m/s

Angle of Attack	Drag Coefficient	Tabulated C_D	Percent Error	Lift Coefficient	Tabulated C_L	Percent Error	y+ Value
0	0.0095	0.0101	6%	-0.0002	0	0.0002*	0.7836
5	0.0124	0.0121	3%	0.4777	0.524	9%	0.7937
10	0.0208	0.0194	7%	0.8968	0.8983	0%	0.8215
14	0.0480	0.094	49%	0.9592	0.8803	9%	0.8201

*This value represents the absolute error rather than the percent error since calculating the percent error would require dividing by zero in this case.

Figures 4.4 and 4.5 show the velocity contour plots at Re = 40,000 and Re = 360,000 for various angles of attack. While FLUENT did not report the correct lift and drag coefficients, the contour plots do show separation resembling the accepted experimental data of Sheldahl et al. (18).

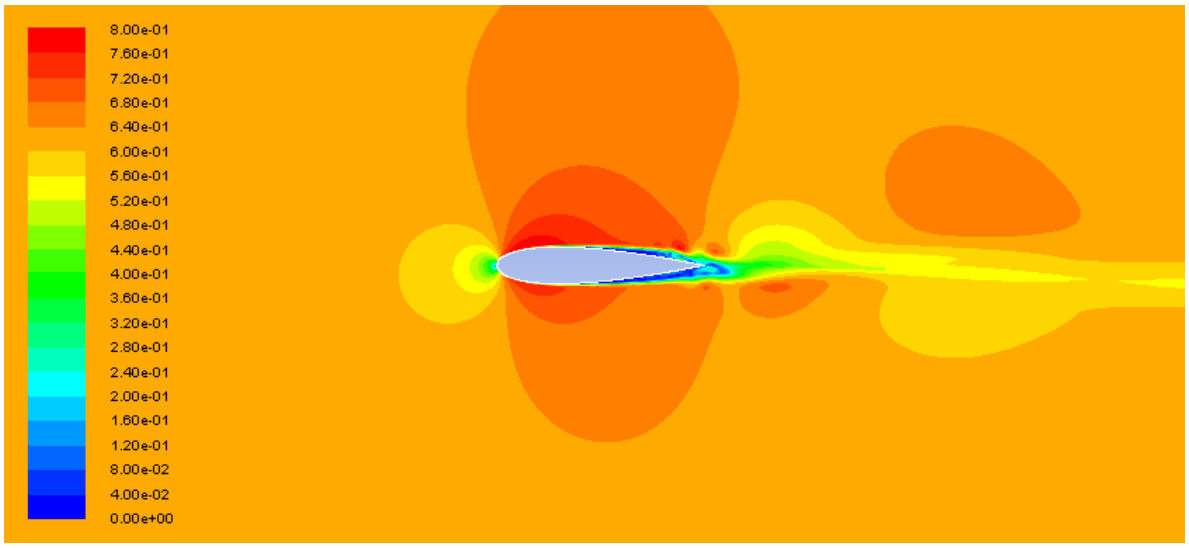

(a) Angle of Attack = 0˚

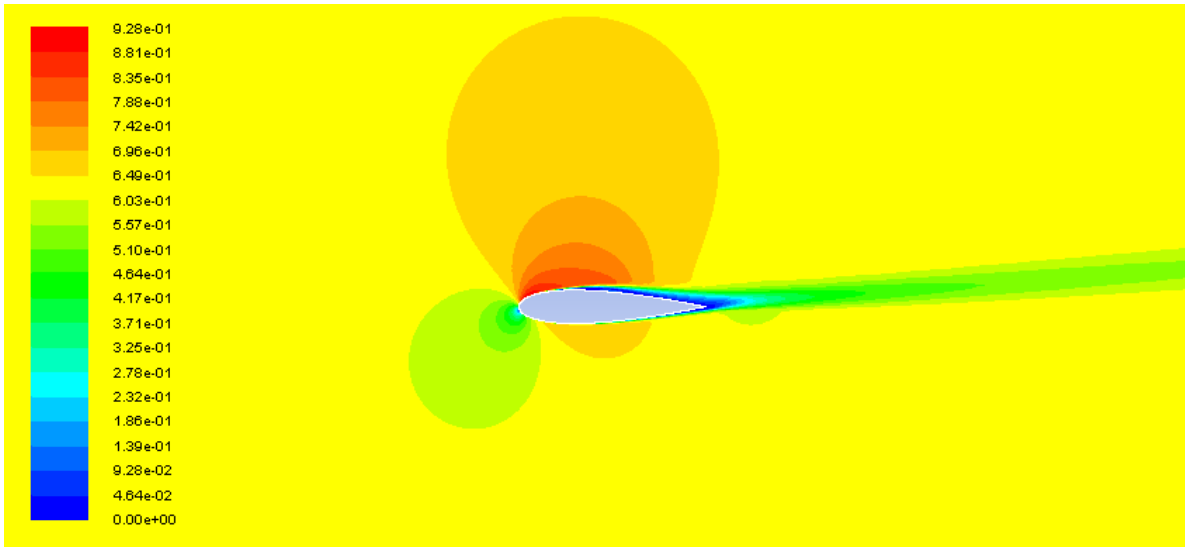

(b) Angle of Attack = 5˚

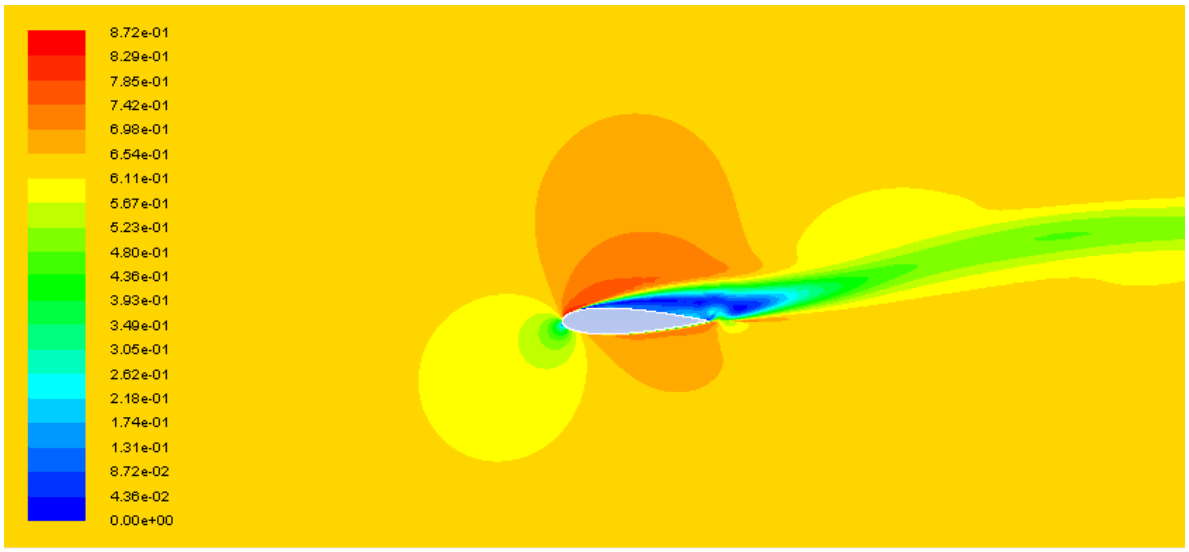

(c) Angle of Attack = 10˚

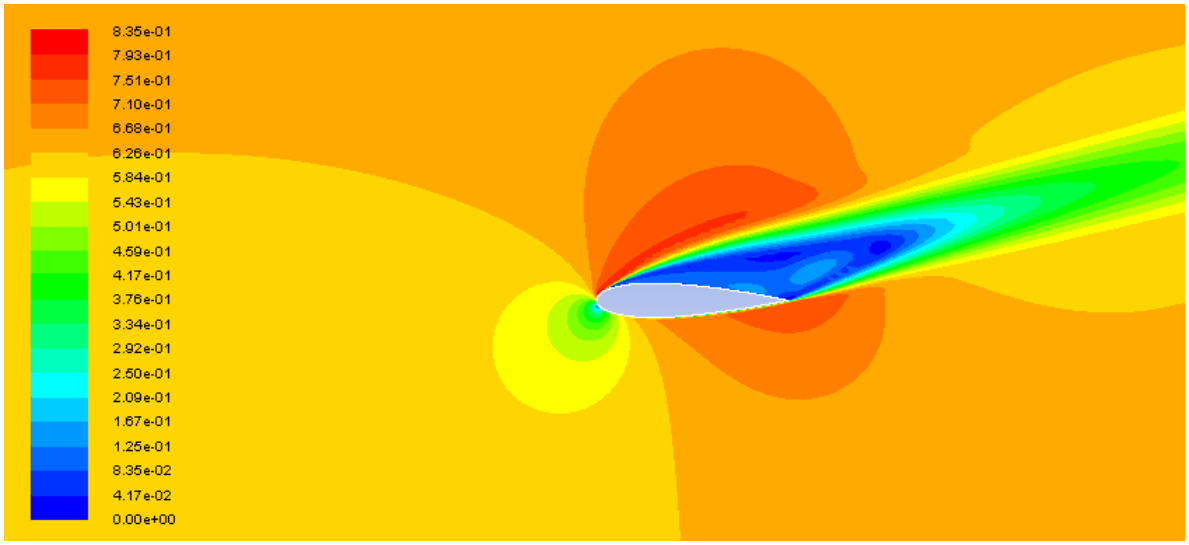

(d) Angle of Attack = 14˚

Figure 4.4. Velocity contour plots for the NACA 0018 airfoil at Re = 40,000 using the Transition SST turbulence model. The modeling software and turbulence models do not accurately capture flow separation. The flow should remain attached (a) when the angle of attack is 0˚, (b) shows an acceptable representation of the flow characteristics, (c) shows separation, (d) shows obvious and experimentally expected separation.

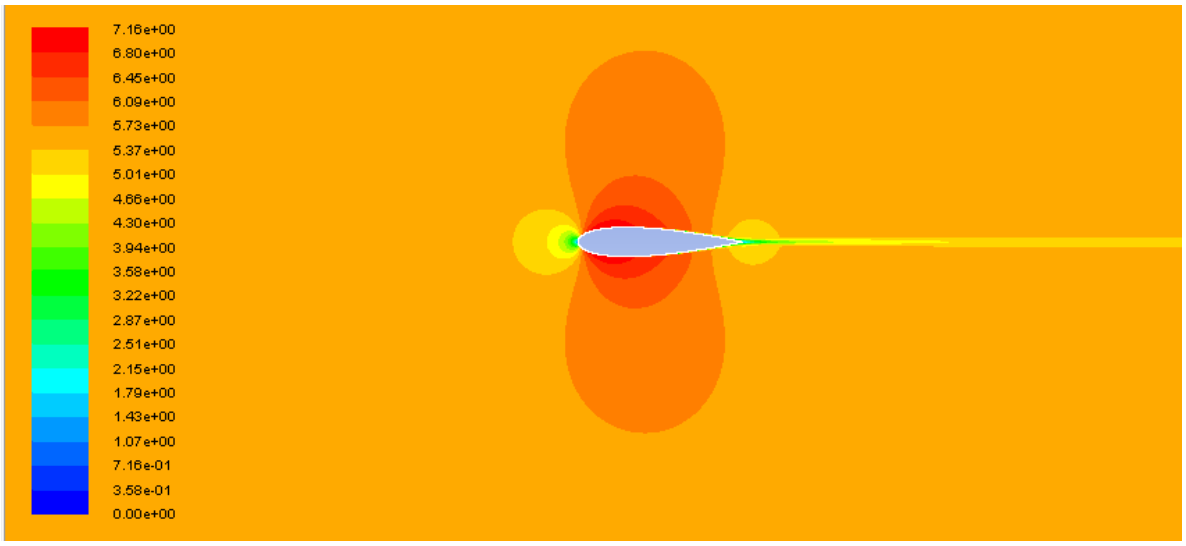

(a) Angle of Attack = 0˚

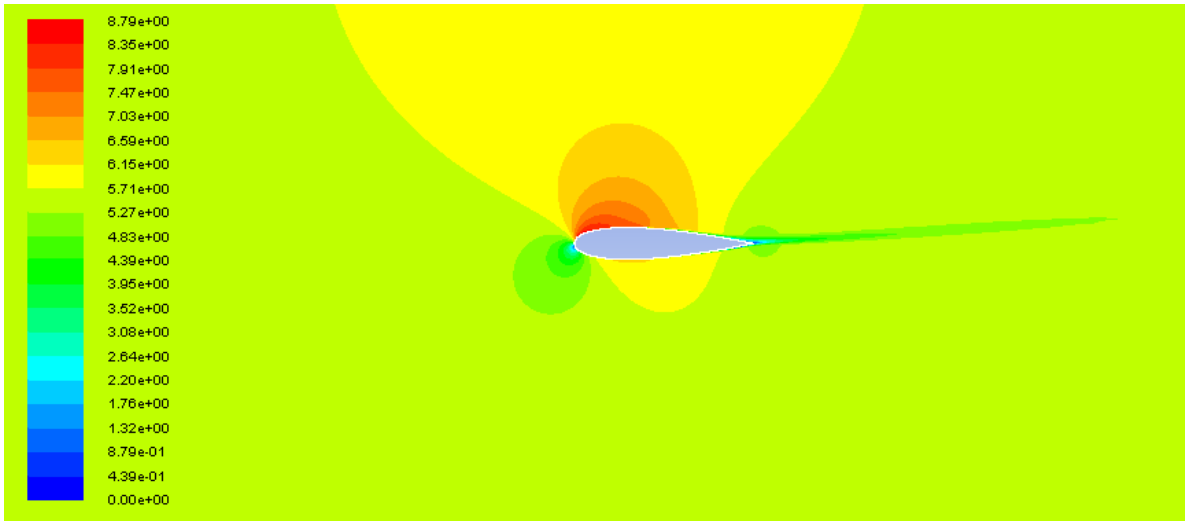

(b) Angle of Attack = 5˚

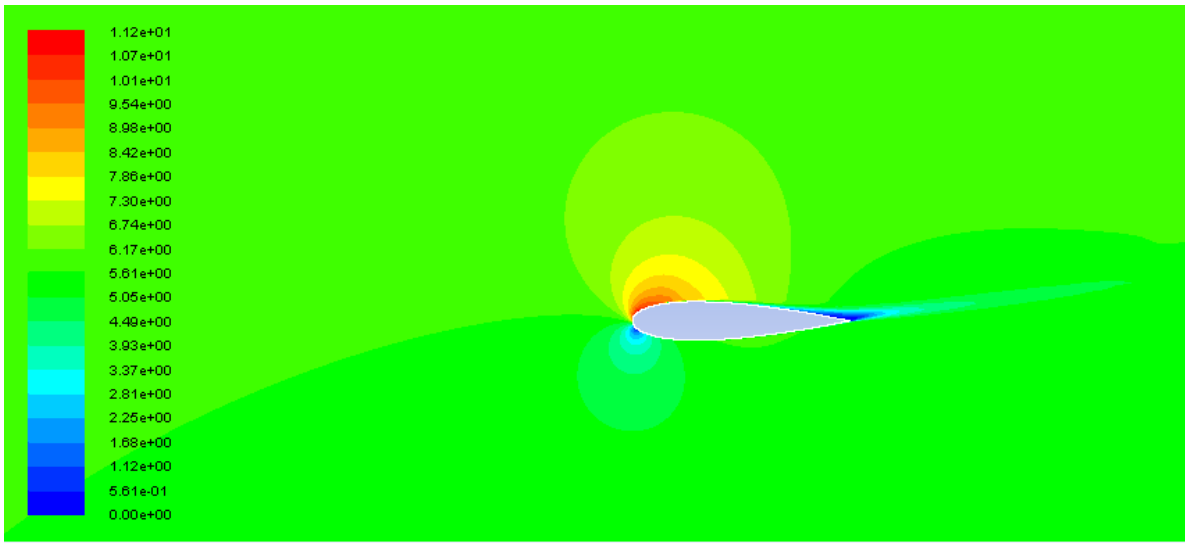

(c) Angle of Attack = 10˚

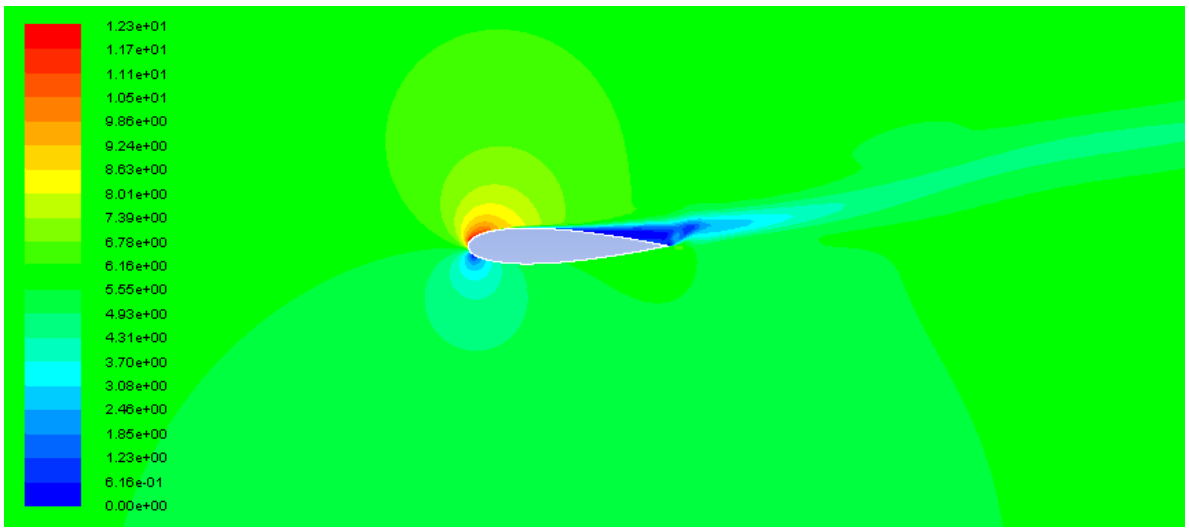

(d) Angle of Attack = 14˚

Figure 4.5 Velocity contour plots for the NACA 0018 airfoil at Re = 360,000 using the Transition SST turbulence model. The drag increases drastically at α = 14˚, the lift value decreases until α = 20˚ before increasing again until α = 50˚, according to Sheldahl et al. (18) Only angles of attack up to 14˚ were simulated at this Reynolds number in this research. Parts (a)-(d) show the expected flow characteristics for the airfoil when Re = 360,000.

The pressure coefficients for the various angles of attack when the Reynolds number is 40,000 and 360,000 are shown in Figures 4.6 and 4.7 respectively. The

pressure distributions for the simulations when Re = 360,000 conform more closely to the shapes of accepted data (38).

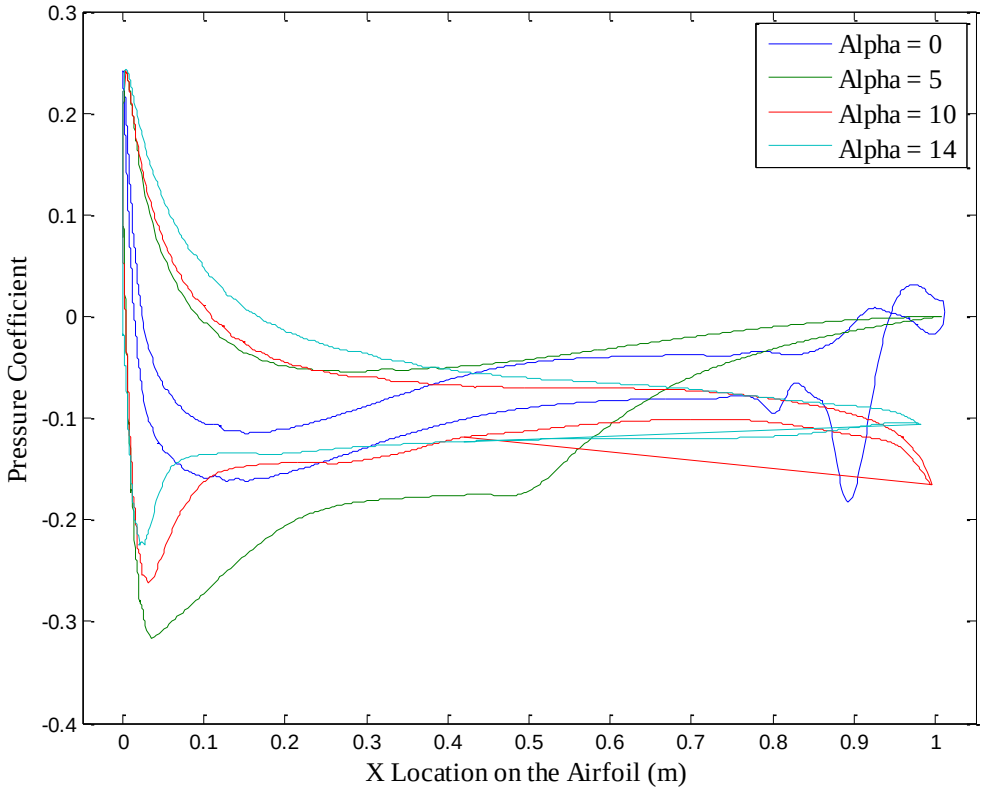

Figure 4.6. Pressure coefficients along the NACA 0018 airfoil for various angles of attack at Re = 40,000

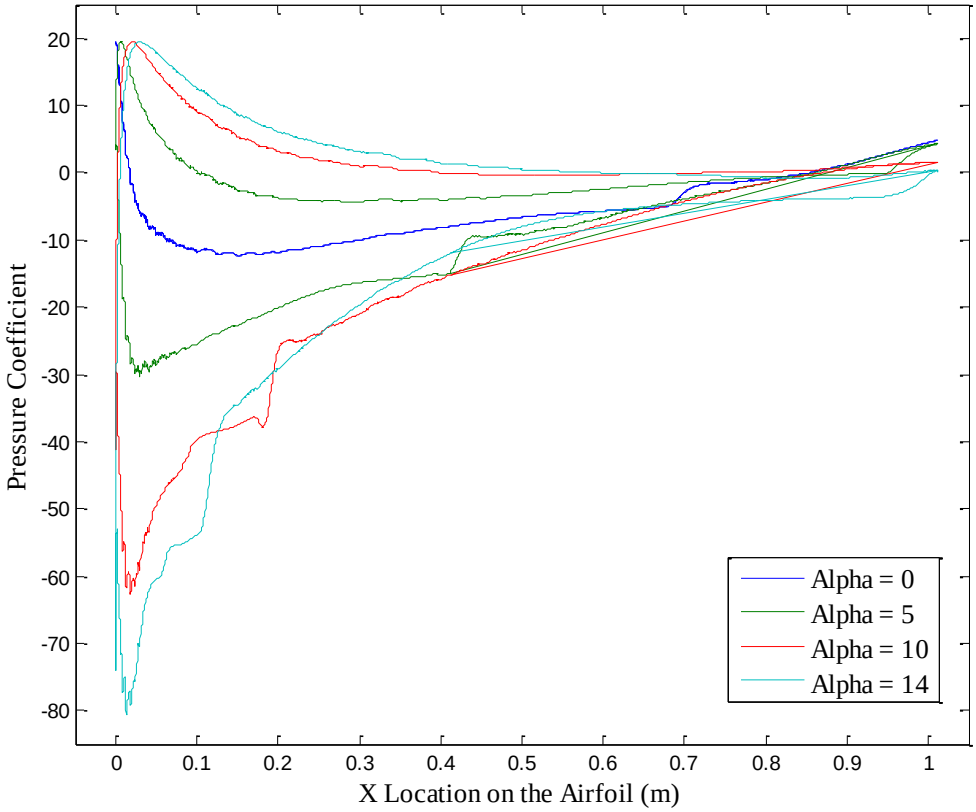

Figure 4.7. Pressure coefficients along the NACA 0018 airfoil for various angles of attack at Re = 360,000

Comparisons between lift and drag coefficients and angles of attack at Re = 40,000 and Re = 360,000 show that there is less error involved with the higher Reynolds number calculations. The lift coefficient versus the angle of attack is given in Figure 4.8. Figure 4.9 shows the drag coefficient as a function of the angle of attack. Figure 4.10 shows the lift coefficient versus the drag coefficient, and Figure 4.11 shows the aerodynamic efficiency (C_L/C_D) versus the angle of attack.

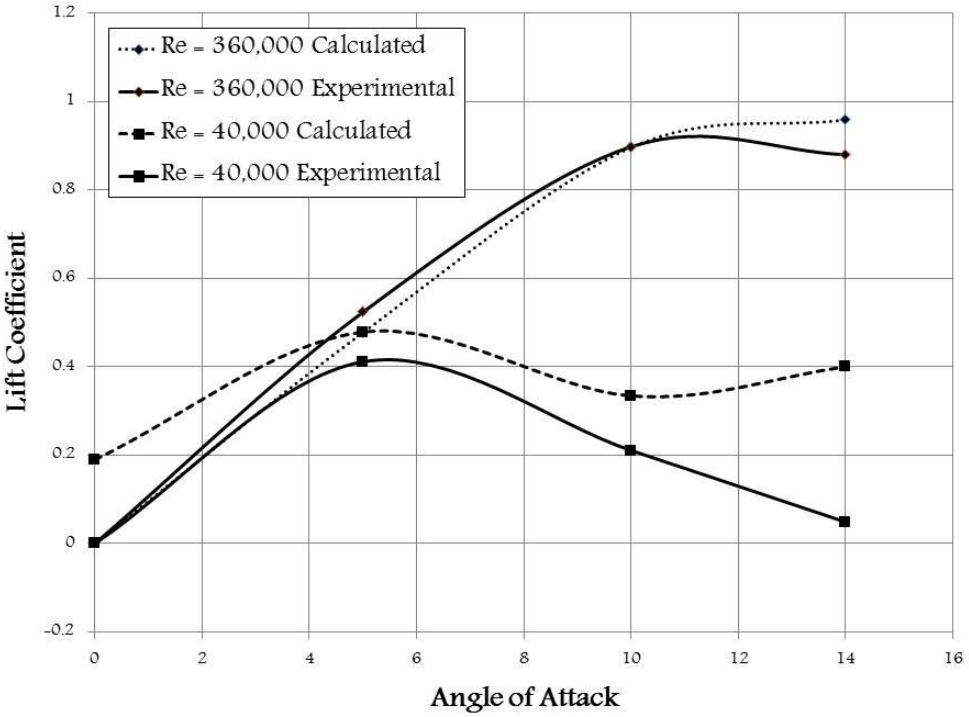

Figure 4.8. Lift coefficient as a function of angle of attack. The higher Reynolds number calculations show much more accurate results.

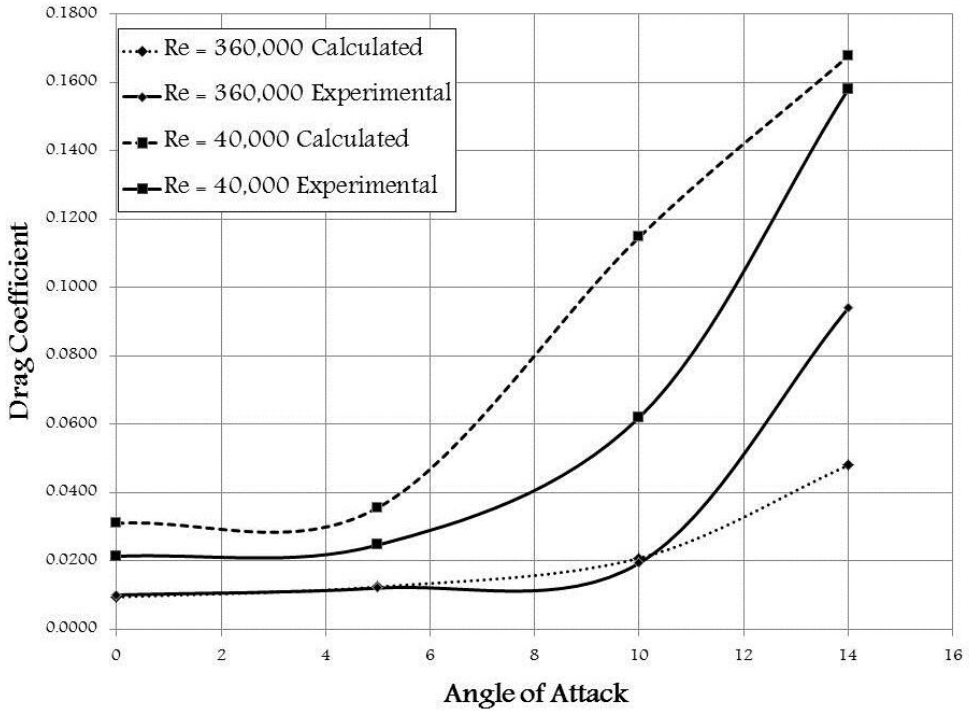

Figure 4.9. Drag coefficient as a function of angle of attack. The higher Re values are still more accurate than the lower Re values.

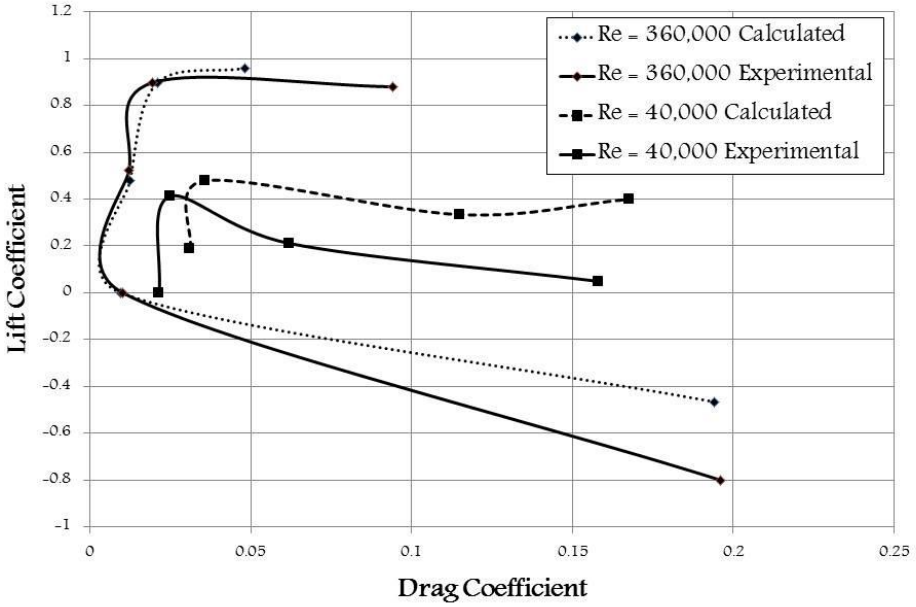

Figure 4.10 Lift coefficient as a function of drag coefficient.

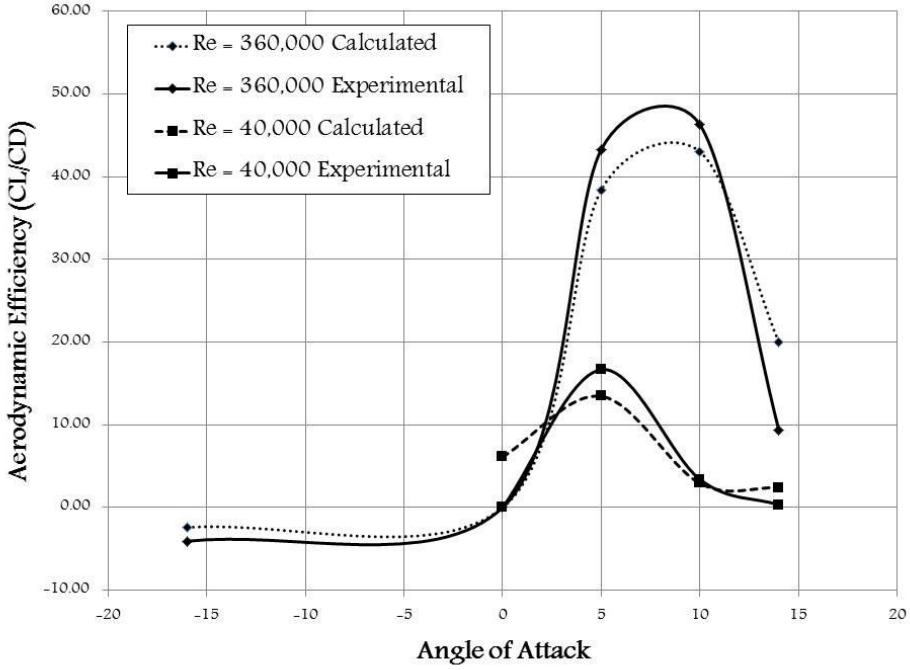

Figure 4.11. Aerodynamic efficiency as a function of angle of attack.

4.3 Two-Dimensional CFD Modeling of the Complete VAWT Design

The complete VAWT design consists of six NACA 0018 airfoils spaced 60˚ apart as shown in Figure 4.12. The goal for simulating this model is to determine the flow characteristics of the turbine and the potential power output from a VAWT designed this way.

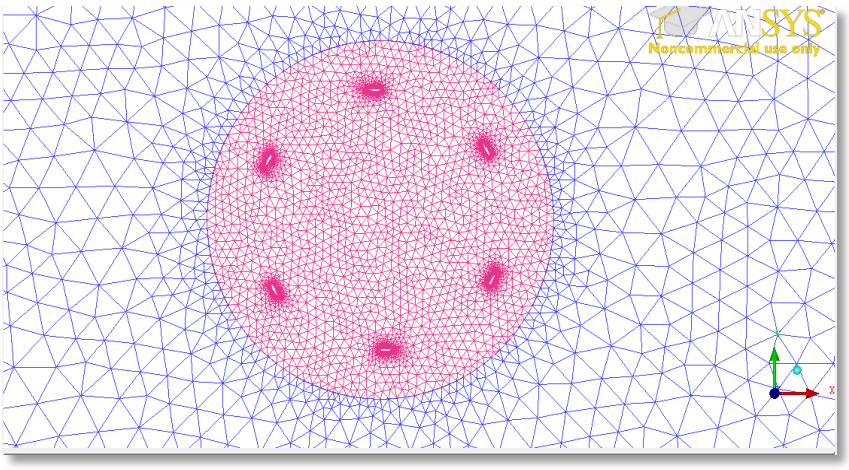

Figure 4.12. Close-up view of the VAWT model. The extent of the farfield is not shown because if it were one could not distinguish the airfoils within the nearfield.

The first step in performing the CFD analysis is a grid refinement study using the transition SST model. The results of the steady state simulation remained the same for numbers of nodes greater than 63,107. Table 4.5 shows the results of the grid refinement study.

Table 4.5 Overall Lift and Drag Coefficients for Various Mesh Sizes at an Angle of Attack of -4˚

Number of Nodes	Overall C_L	Overall C_D	Y+ Value
38660	-0.0534	0.3579	3.634
63107	-0.0651	0.3638	0.8821
84495	-0.0662	0.3624	0.5220

The values for the overall C_L and C_D do not change much past 63,107 nodes, so it is the most computationally efficient number of nodes. The y+ values vary using the mesh with 63,107 nodes as different tip speed ratios are examined using a steady-state rotating nearfield. To maintain accuracy a y+ value less than one is always maintained by adapting the mesh when necessary. However, the use of a steady-state simulation provided unreasonable results, so a transient simulation with a sliding mesh technique to simulate the motion of the turbine was employed instead.

The sliding mesh technique was used to simulate the rotational motion within the nearfield. To use the sliding mesh technique, the simulation needs to be run as a transient calculation. This allows the user to enter the rotational velocity into the "Mesh Motion" section in FLUENT, which causes the nearfield mesh to rotate at the specified radial velocity when the transient simulation is run. The boundary conditions are shown in Figure 4.13. As shown in this figure, the model consists of the cross-section of the turbine (the six blades represented by airfoils), a nearfield which can be rotated when used in a rotating-steady-state analysis and the farfield. A large simulation domain allows for modeling without the effects of solid blockage from the walls.

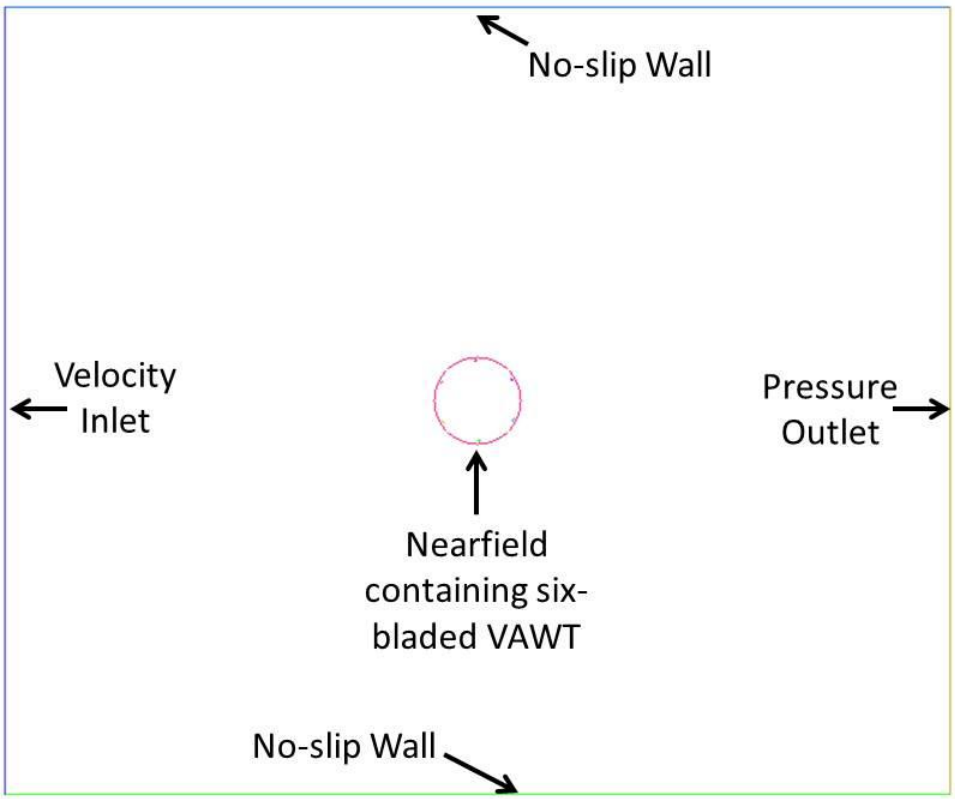

Figure 4.13. Boundary conditions for the VAWT simulation. The nearfield contains everything within the circle in the center of the figure, and the farfield is everything outside of the circle.

4.3.1 Analyzing the Simulations of the VAWT

While the steady-state calculations did not give useful output to characterize the vertical axis wind turbine, the transient models provide more realistic information. FLUENT was used to rotate the nearfield of the VAWT to simulate different tip speed ratios and learn about the effects of these variations on the forces acting on the blades. Figure 4.14 shows the forces acting on each blade and number of the blades for use in future discussions. The lift force is designated F_L, the drag force is F_D, the tangential force if F_T, and the normal force is F_N. The lift force is always perpendicular to the incoming wind velocity, and the drag force is always parallel to the incoming wind

velocity. The normal and tangential forces are relative to each blade and are perpendicular to the blade's chord and parallel to it, respectively.

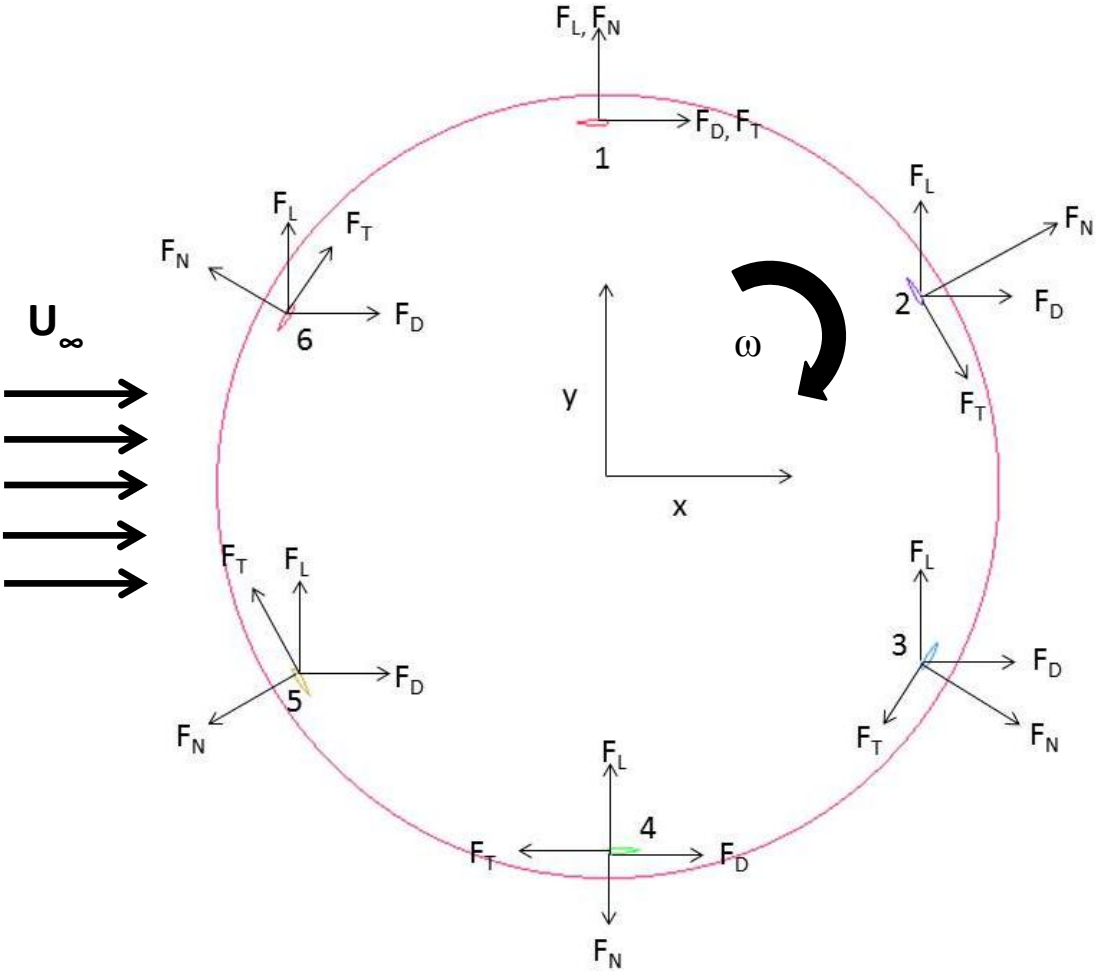

Figure 4.14. Force distribution on each of the six wind turbine blades. F_L acts normal to the incoming wind, F_D acts parallel to the incoming wind, F_T acts parallel to the blade's chord and F_N acts normal to the blades chord.

The sliding mesh allows for rotation of the nearfield and the blades in the simulation to experience the rotational forces while performing a transient response.

4.3.2 Results from the Simulations of the VAWT

In order to calculate the power, the torque must first be calculated for each blade, then added together to get the total torque. The torque on each blade is calculated using Equation 5, and summed to get the total torque, T.

$$T_i = F_{Ti}R \quad \text{for i=1,…6} \tag{5}$$

Equation 6 describes how the mechanical power is calculated for the vertical axis wind turbine,

$$P = T\omega \tag{6}$$

Then, using the power calculated from Equation 6, the power coefficient, C_P, is calculated as shown in Equation 7,

$$C_P = \frac{P}{\frac{1}{2}\rho A U_\infty^3} \tag{7}$$

where ρ is the density of air, ρ = 1.225 kg/m^3, and A is the swept area of the wind turbine, given in Equation 8 for its elliptical shape in this case, and U_∞ is the free stream velocity. The area is given by,

$$A = \pi \frac{H}{2}\frac{D}{2} \tag{8}$$

where H is the turbine height, 3.2 m, and D is the turbine diameter, 1.874 m, such that the swept area is equal to 4.7 m^2. Equations 4-7 are used to calculate the power coefficient for various tip speed ratios.

Based on the literature and results of Migliore et al. (41) the coefficient of performance decreases for lower solidity ratios. The solidity, σ, of a wind turbine is equal to NC/R, where N is the number of blades, C is the chord length, and R is the radius of the wind turbine (19). Turbines with a larger number of blades have a larger solidity. The solidity of the turbine modeled here was 56%. Turbines with lower solidity peak later and

have lower coefficients of performance. The plot showing all this information is reproduced from Migliore et al. (41) in Figure 4.15.

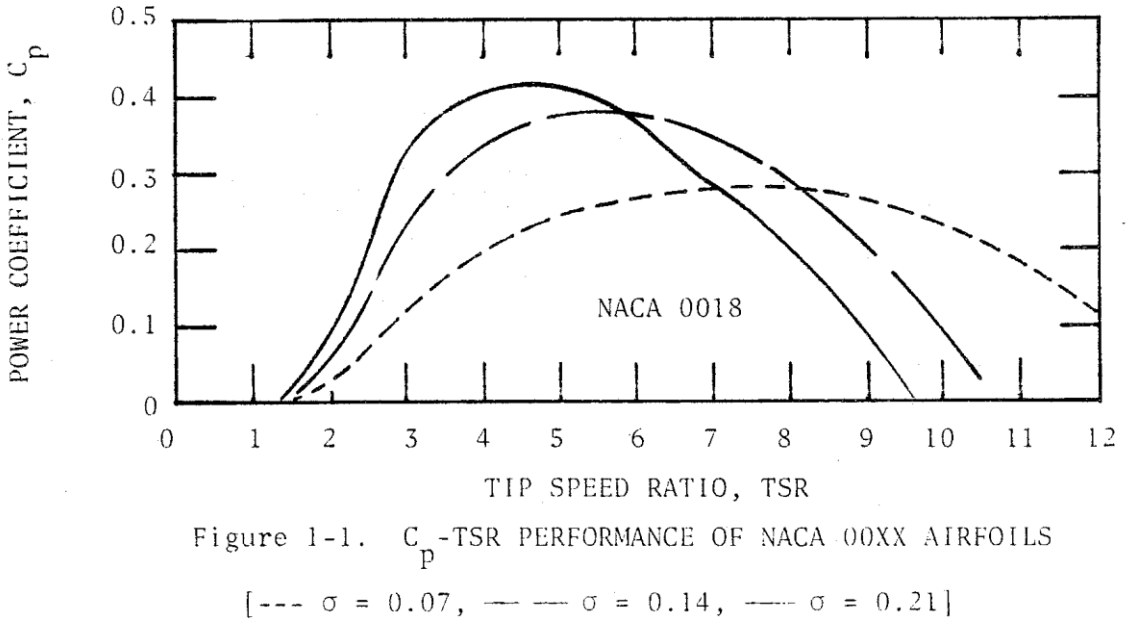

Figure 4.15 Power coefficient vs. tip speed ratio graph from Migliore et al. (41). They tested vertical axis wind turbines with two blades to get this data which shows that turbines with larger solidity peak early and can reach power coefficients close to 0.4.

Paraschivoiu stresses that small inaccuracies in the modeling of the lift and drag coefficient can produce large differences in power and torque (42). As the results from section 4.2.3, “Results from Airfoil Validation,” show, there are prominent differences between the modeled and experimental lift and drag coefficients, especially at lower Reynolds numbers. While additional iterations and refinement of the sliding mesh technique are required to validate this computational model, preliminary results correspond to the expected results based on the trends of solidity on the performance coefficient. A graph of the power coefficient versus tip speed ratio is shown in Figure 4.16. Further evaluation of this modeling technique is ongoing.

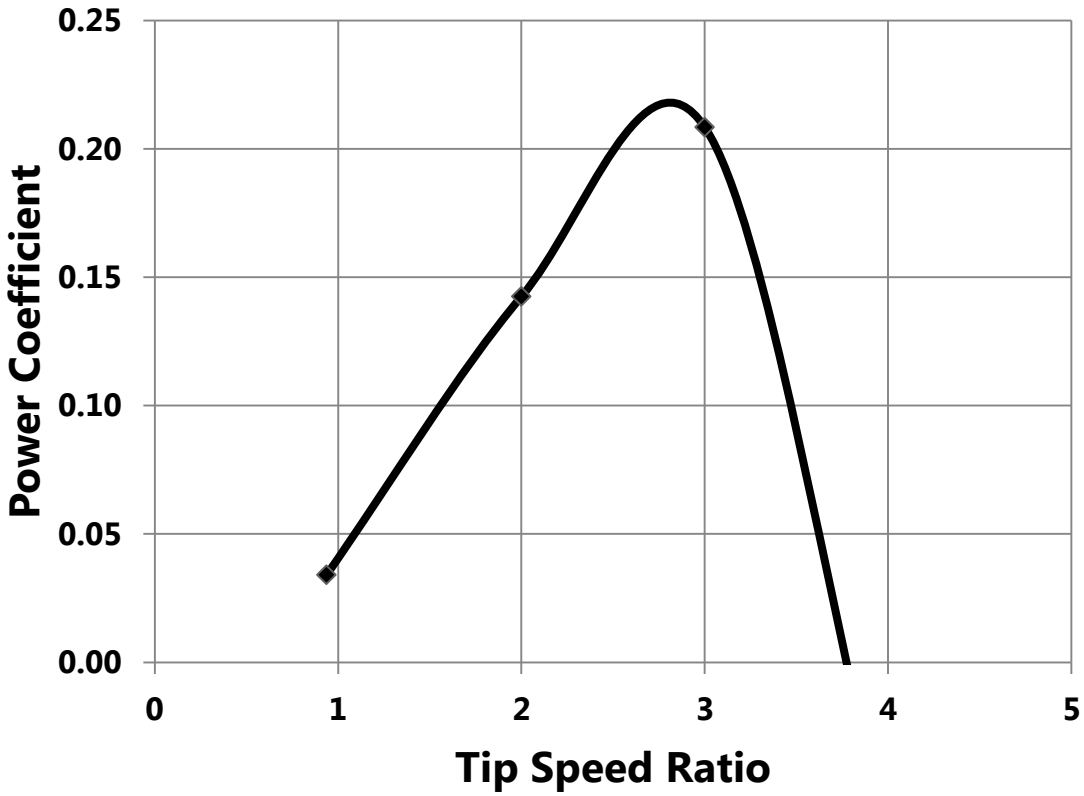

Figure 4.16 Power coefficient versus tip speed ratio for the vertical axis wind turbine.

Figure 4.16 estimates that a peak power coefficient will occur at a tip speed ratio near 2.8 and will reach about 22%. Since no other vertical axis wind turbine data has been found which tests a turbine with six blades, the data presented here is accepted as realistic since it follows the trends from solidity effects. Experimental testing will provide additional support for this computational model.

4.4 Conclusions and Recommended Work on the Vertical Axis Wind Turbine

Low Reynolds number modeling of the vertical axis wind turbine proved to be a challenging task and the literature review showed that other researchers have also found inaccuracy in prediction. This illustrates the dire need for more accurate turbulence

modeling and deeper research towards solving of the Navier-Stokes equations under low Reynolds number conditions.

The transition SST model proved to be the most accurate in modeling of the NACA 0018 airfoil characteristics. For the vertical axis wind turbine, steady-state simulations proved inaccurate and the transient sliding mesh technique improved the force, torque, and subsequently power calculation accuracy. Using this method, a peak power coefficient of 22% was reached for the six-bladed vertical axis wind turbine at a tip speed ratio of 2.8. Further exploration of low-Reynolds number turbulence modeling is recommended to overcome the mismatch between the computational and experimental results.

5 TUBERCLES TO ENHANCE THE AERODYNAMIC EFFICIENCY OF WIND TURBINE BLADES

Bio-inspired technology is increasing in popularity and showing promise for solving many complex problems. In the aerospace field, researchers are developing seagull-inspired wings to increase stability and agility in planes. Acoustic engineers use bats to develop sonar systems and structural engineers have been using the honeycomb that bees make as an example when designing lightweight wall structures (43). The focus of this chapter is on exploring the use of tubercles, like those found on a humpback whale, to increase the stall angle of aerodynamic blades. Figure 5.1 shows a photograph of the tubercles on a humpback whale's fin taken from Fish et al.'s paper (23).

Figure 5.1 Tubercles on humpback whales' flippers (23).

Various researchers including van Nierop (5), Miklosovic, Fish, and Swanson have found that tubercles delay the angle of attack at which stall occurs, and produce a

higher aerodynamic efficiency ($C_L/C_{D,}$ where C_L is the lift coefficient and C_D is the drag coefficient). Not all whales have tubercles; in fact, humpback whales are the only example that use tubercles for more efficient maneuverability and the capture of prey (23). Tubercles on the leading edge of a model wing have proven to increase the lift throughout higher angles of attack and decrease drag (25). This means that stall occurs at higher angles of attack and could allow for better performing wind turbine blades. This is especially effective for smaller-scale wind energy generators that operate at lower Reynolds numbers (~ $\leq$ 200,000) because at larger Reynolds numbers, the tubercles have been found to accelerate the onset of cavitation (23). This chapter introduces the ability of the tubercles to increase the efficiency of a small-scale (440 mm or 17.3 in) wind turbine blade. This chapter is not intended to be a detailed analysis of the technology but an overview of this topic.

5.1 Problem Description and Goals

The base for the comparison of the straight blade to one with tubercles begins with a RISO-A-15 airfoil used to create 440 mm (17.3 in) long blades. The first design is a straight tapered blade shown in Figure 5.2, and the second is a tapered blade with leading edge tubercles. In the tubercle blade design, there are 10 tubercles along the blade's leading edge as shown in Figure 5.3. The goal of this effort was to explore the concept of using tubercles to enhance the lift and drag characteristics of the blades.

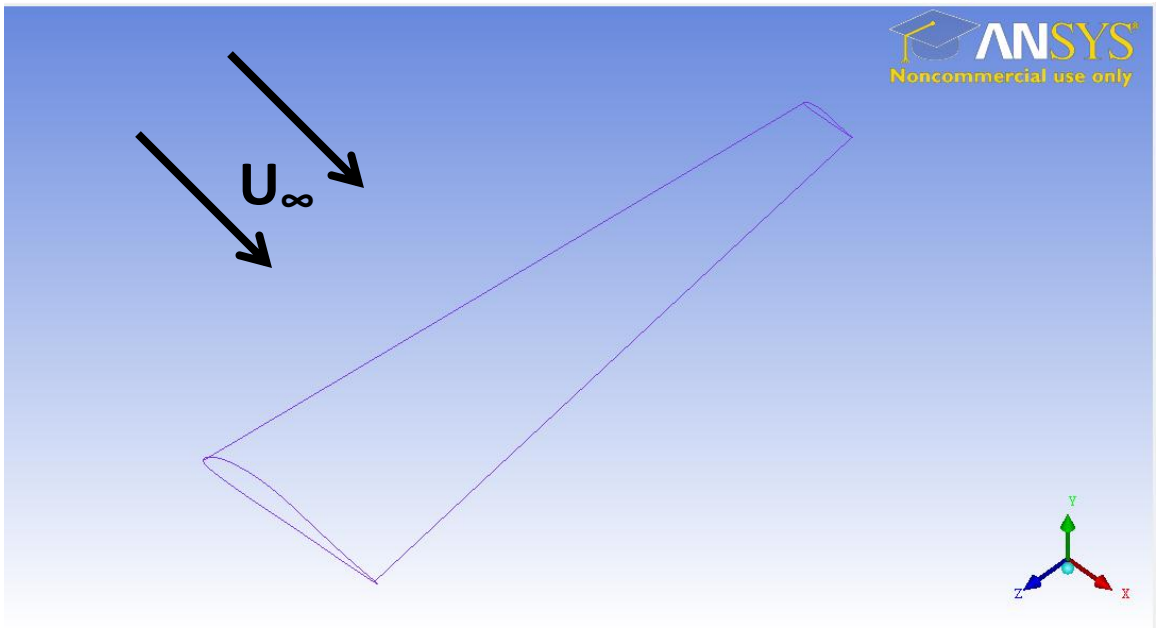

Figure 5.2. Straight blade extruded from a RISO-A-15 airfoil.

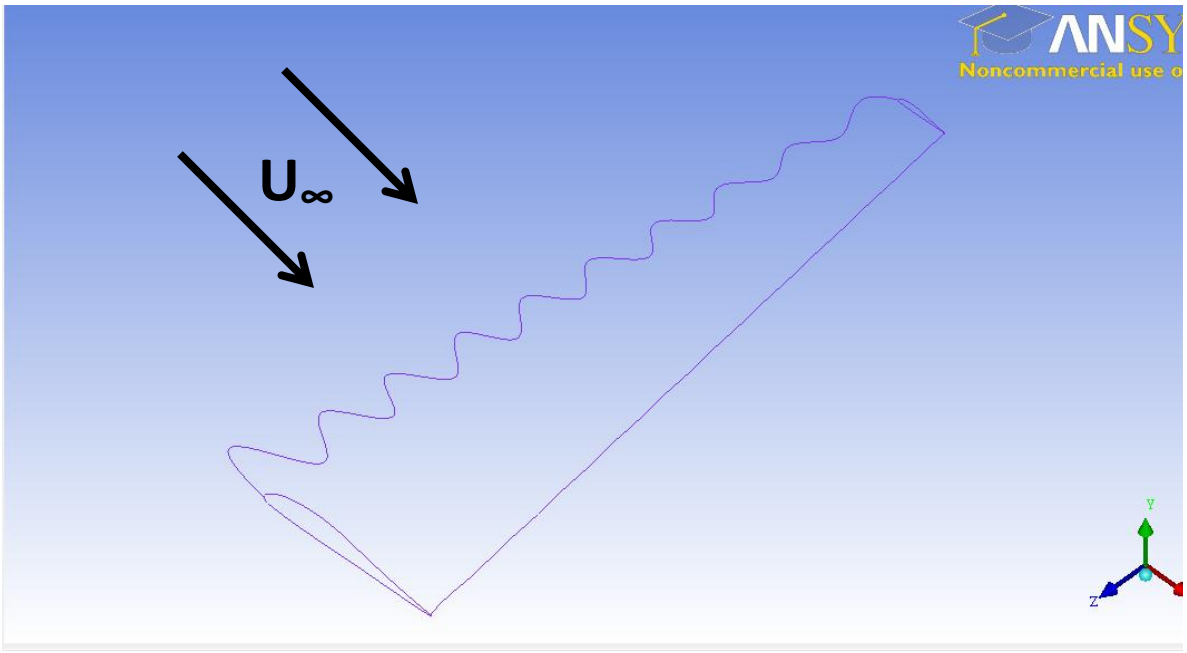

Figure 5.3. Blade with leading edge tubercles. This blade was also extruded from a RISO-A-15 airfoil.

5.2 Performance Comparison between Blades With and Without Leading-Edge Tubercles

Fish et al. found that blades with tubercles 4% of the chord length can increase lift by 4.8%, decrease drag by 10.9%, and increase the lift to drag ratio by 17.6% when tested at a 10° angle of attack (23). Low Reynolds number wind tunnel data has not been found for the RISO-A-15 airfoil, but the goal through experimental and computational efforts was to validate Fish et al.'s claims for small-scale wind turbine blade applications.

Blades have been fabricated and tested in the Virginia Tech's wind tunnel. Figure 5.4 shows the fabricated blades. They are of the same size as the modeled blades (440 mm (17.3 in)). Physical testing has occurred once in the wind tunnel, but since wind tunnel time is expensive, computational models were created to estimate the physical characteristics of the blades with tubercles for future testing.

(a) (b)

Figure 5.4 Experimental blades: a) straight blade, b) blade with tubercles

The Virginia Tech wind tunnel has the dimensions 1.83 m x 1.83 m, and has an turbulence intensity of 0.05% or less (47). Wind tunnel testing at wind speeds of 4.5 m/s, 5 m/s, and 5.5 m/s showed that tubercles do enhance the performance coefficient of the

blades. These wind speeds correspond to Reynolds numbers between 126,000 and 154,000. Figure 5.5 and 5.6 show the power coefficient versus tip speed ratio for the straight blades and the blades with tubercles respectively. The blades with tubercles provide a 2% increase in power coefficient. Once a few promising results have been obtained using CFD, the wind tunnel testing can be used to validate the hypothesis. This will not only save time and money but also provide physical explanation for the observed behavior.

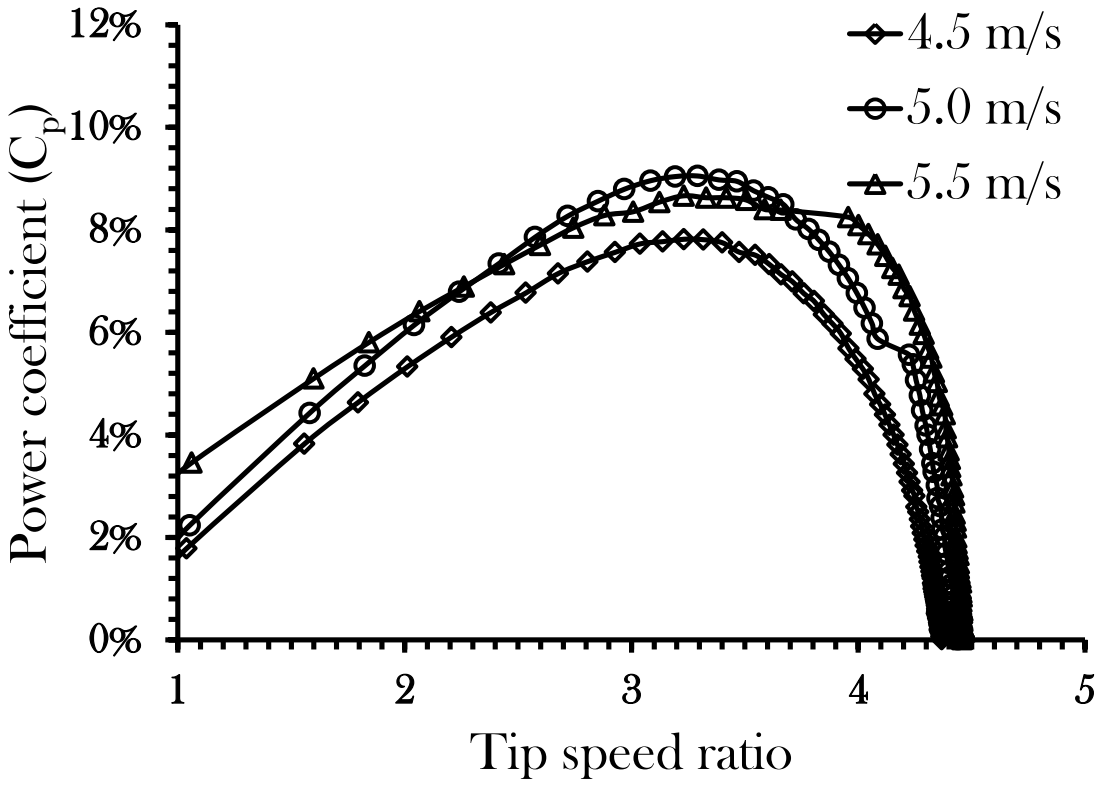

Figure 5.5 Power coefficient versus tip speed ratio for blades without tubercles.

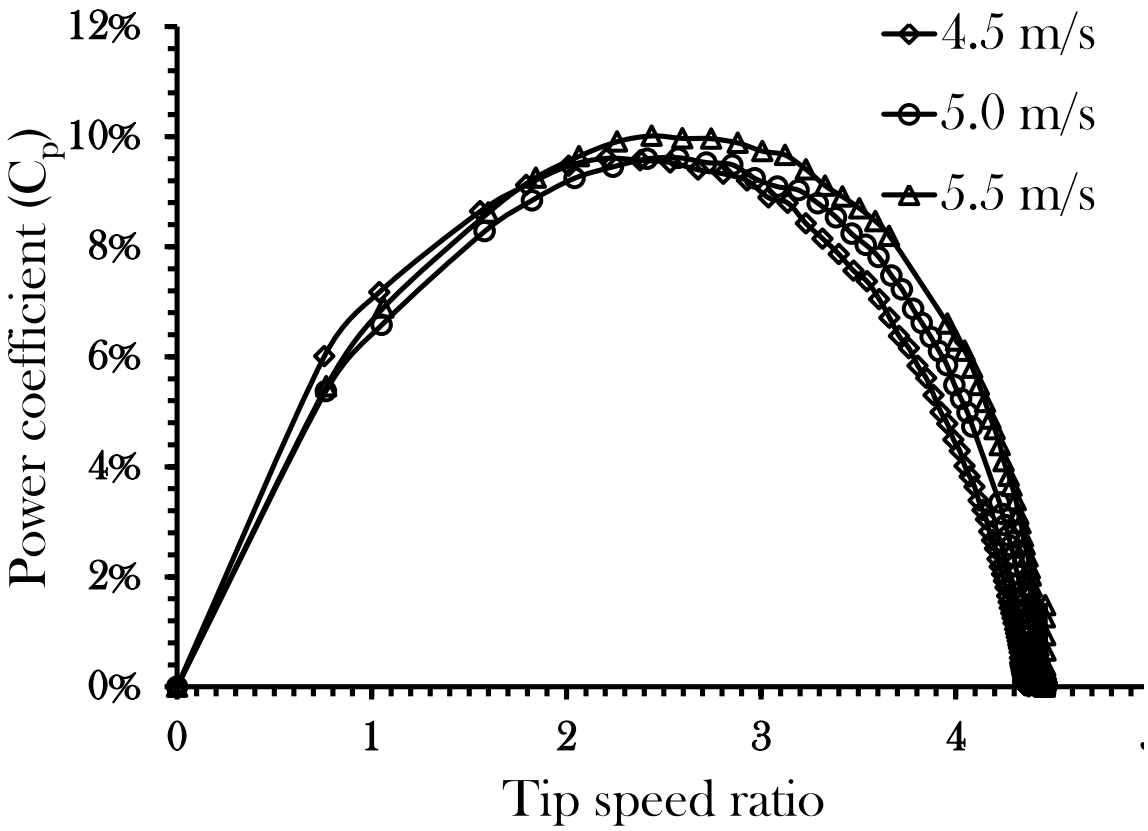

Figure 5.6 Power coefficient versus tip speed ratio for blades with tubercles.

5.3 Three-Dimensional Model and Mesh of Blades with Tubercles versus Straight Blades

The three-dimensional models were meshed using ANSYS's meshing software, ICEM. A 3D unstructured mesh was created around a model of the straight blade and a model of the blade with tubercles along the leading edge. Both models use the same airfoil, the RISO-A-15 and had the same length and taper. The only difference between them was the addition or omission of tubercles. Figures 5.7 and 5.8 show the meshes of the straight blade and the blade with tubercles, respectively.

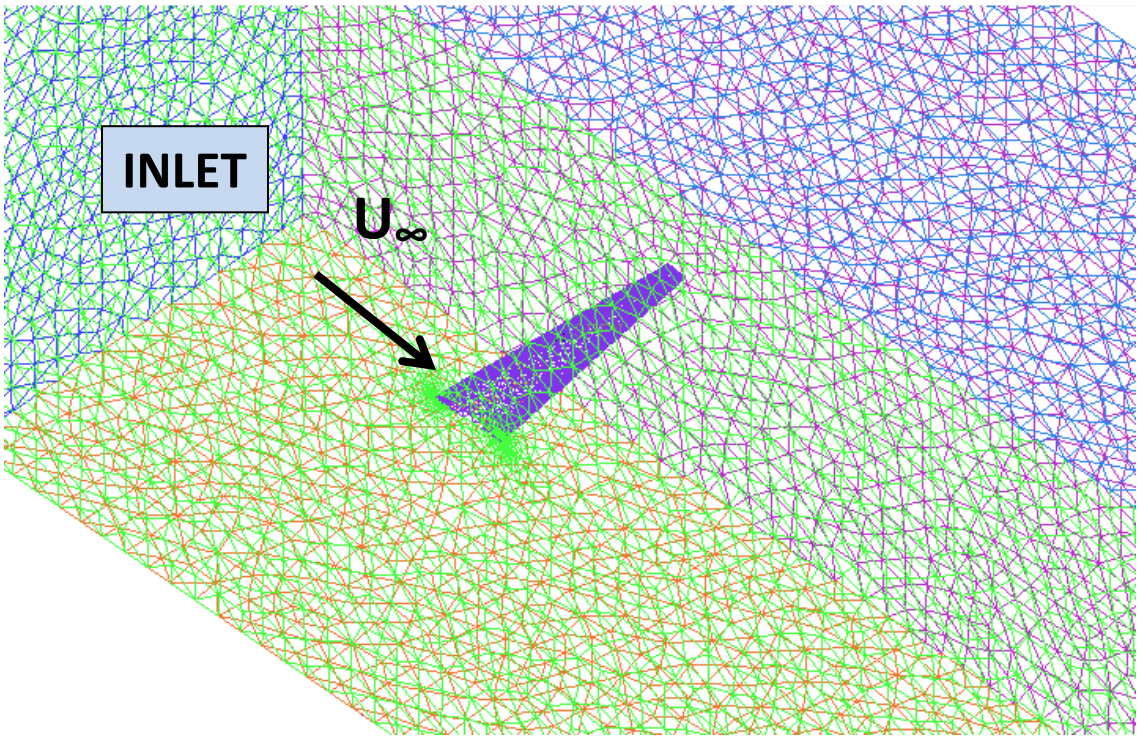

Figure 5.7 3D meshing of the straight blade for comparison to the blade with tubercles.

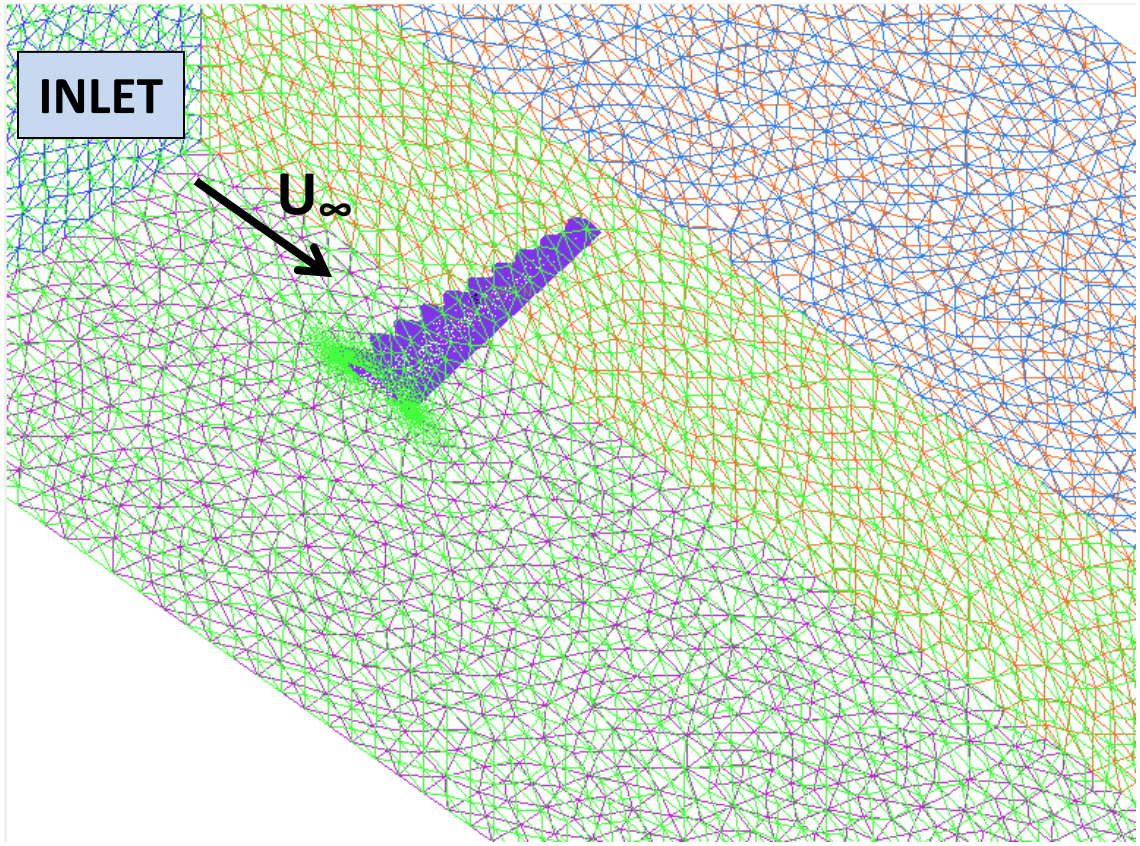

Figure 5.8 3D meshing of the blade with tubercles

Three-dimensional modeling using the k-ω SST turbulence model has proven computationally expensive and also inconclusive at this point. Weber et al. (48) has determined that RANS models can cause inaccurate results for the lift and drag forces, especially for low Reynolds number effects. Thus, exploration of Detached Eddy Simulation (DES) or Large Eddy Simulation (LES) models is recommended. The LES model, while most computationally expensive, would most accurately represent the flow physics involved in the low Reynolds number simulation of the blades with and without tubercles. The LES model is limited to Reynolds numbers on the order of $10^4 \sim 10^5$ due to the fact that the eddies become small near the wall and require Reynolds number dependent solutions (46); the data being modeled here fits the criteria nicely.

Detached Eddy Simulation, which combines the LES model for separated regions and the unsteady Reynolds Averaged Navier Stokes (RANS) model in the boundary layer (46), has provided accurate results as shown by the study of Pedro and Kobayashi (49). This model is less computationally expensive than the LES model. However, the DES model was developed for high Reynolds number flows (46) and this should be taken into account. If computational power is sufficient the LES model would be the most appropriate for these simulations.

5.4 Conclusions and Future Work

Researchers have recently found that blades with tubercles perform better than blades without them (5, 23, 25, 26). No other experiments from the literature have been run at the 1 m (3.28 ft) diameter rotor scale for wind turbine blades using this feature. Models have been created to evaluate the effects of the use of tubercles to enhance blade characteristics and wind tunnel tests show a 2% increase in power coefficient when

blades with tubercles are used. These tests were performed at wind speeds of 4.5 m/s, 5 m/s, and 5.5 m/s. Models have been created for simulation using CFD, but reasonable results have not been produced using the k-ω SST model. Additionally, the computational expense of simulating the 3D model is quite high. More appropriate turbulence models have been discussed and recommended.

6 CONCLUSION

To fabricate the small-scale wind that is worth the upfront installation costs, increased efficiency is necessary. This thesis explored three aspects of small scale wind: diffusers to augment the velocity at the rotor, tubercles to enhance the aerodynamic efficiency, and vertical axis wind turbines designed for simpler installation and maintenance. The main focus in the research was to identify the features that could lead to increased power output.

Well-designed diffusers were found to increase the power output up to four times for wind speeds less than 4.47 m/s (10 mph). Such wind speeds are typical of residential altitudes and applications. Using statistical analysis, the amplification factor was found to depend on the length of the inlet and outlet of the diffuser, and the angle of each as well. As the inlet wind velocity increases, so does the velocity amplification factor. Since power is proportional to velocity cubed, it increases significantly for even small increases in velocity.

Vertical axis wind turbines are also an area of increased interest for small-scale wind energy generation. Wind turbines using airfoils of 0.08732 m (3.44 in.) chord length were simulated; however, more research is necessary in understanding and modeling turbulence at low Reynolds numbers. Commercial fluid dynamics modeling packages were unable to correctly report lift and drag coefficients comparable to that of accepted experimental data regardless of various modeling strategies. A review of literature was included to support the need for more research to address the turbulence problem. The peak power coefficient for the six-bladed VAWT was found to be 22% at a tip speed ratio of 2.8.

Another efficiency enhancing opportunity for horizontal axis wind turbines is to use leading-edge tubercles to enhance the aerodynamic efficiency of the blades. Blades were created analytically and tested experimentally. Experimental models showed a 2% increase in power coefficient when tubercles were used rather than straight-edged blades. Analytical models are being examined to see if they can be used to estimate the usefulness of the tubercles. Suggestions have been made in this thesis to improve the accurate representation in CFD of the flow physics surrounding the blades with and without tubercles at low Reynolds numbers.

6.1 Fundamental Achievements

The added value of the research presented in this thesis includes strategies for the modeling of small-scale horizontal and vertical axis wind turbines. The first chapter shows the utility of a wind turbine diffuser in amplifying the wind velocity at the turbine. The effect of each of the diffuser's geometrical parameters on velocity amplification factor was quantified. Amplifying the velocity is instrumental in increasing the efficiency of the turbine because power is proportional to velocity cubed. The diffuser research also developed an optimal design for small-scale (1 m diameter (3.28 ft)) wind turbine diffuser.

The research on the vertical axis wind turbine using NACA 0018 airfoils demonstrated the need for better turbulence models at low Reynolds numbers. A review of literature towards modeling vertical axis wind turbines for low wind speed applications was conducted. Results regarding the suitability of the existing methods were obtained with respect to the vertical axis wind turbine. Models of the vertical axis wind turbine

were developed and tested using a transient sliding mesh technique. Prior literature did not have data for six-bladed vertical turbines, so the information presented in this thesis strives to begin filling that gap by presenting a high solidity turbine with the capability of achieving a 22% power coefficient at a tip speed ratio of 2.8.

The testing of tubercles like those found on humpback whales for wind turbines was investigated. These features have yet to be studied for wind turbines in the 1 m (3.28 ft) diameter range. A thorough literature review was conducted to estimate the effects of tubercles on small-scale wind energy conversion systems. The research presented here resulted in development of three-dimensional computational models that can provide the effects of adding tubercles to small-scale wind turbine blades. Experimental data was also presented that showed a 2% increase in power coefficient when blades with leading edge tubercles were used.

6.2 Future Studies

This thesis provides a good basis for future work to be performed in the evolution of small scale turbines. In regard to the diffuser augmented wind turbine, experimental testing and field testing should be performed to experimentally validate the theoretical models developed in this thesis. Refinement and creation of an accurate turbulence model for simulation of the vertical axis wind turbine performance characteristics is an important area to study so that future researchers can accurately model low Reynolds number conditions. Further investigation of the number and orientation of blades for this specific vertical axis wind turbine design could help in understanding the different configurations and capabilities of the wind turbine and in determining the optimal amount

of blades. Three-dimensional computational and experimental modeling of the straight blades and blades with tubercles could be used to quantify the enhancements possible through the use of tubercles on the leading edge of small-scale wind turbine blades for low-altitude and low wind speed applications.

References

[1] Vanek, F.M, Albright, L.D., and L. T. Angenent, Energy Systems Engineering: Evaluation and Implementation, McGraw Hill, New York, NY, Chap. 1, 2012.

[2] Goggin, M. (AWEA), "The Facts about Wind Energy and Emissions," Renewable EnergyWorld.com, 2010, http://www.renewableenergyworld.com/rea/news/article/2010/09/the-facts-about-wind-energy-and-emissions

[3] Foreman, K.M., and B.L. Gilbert, "Further Investigations of Diffuser Augmented Wind Turbines* Part I – Executive Summary, Report RE – 585 for the U.S. Department of Energy Division of Solar Energy Federal Wind Energy Program, Bethpage, NY. 1979.

[4] Whittlesey, R.W., Liska, S., and Dabiri, J.O. "Fish schooling as a basis for vertical axis wind turbine farm design." J. Bioinspiration and Biomimetics, Vol. 5, 2010. DOI: 10.1088/1748-3182/5/3/035005

[5] Van Nierop, E.A., Alben, S., and M.P. Brenner, "How Bumps on Whale Flippers Delay Stall: An Aerodynamic Model," Physical Review Letters, Vol. 100, 2008

[6] Wind Powering America, "Installed Wind Capacity," U.S. Department of Energy, 2013, < http://www.windpoweringamerica.gov/wind_installed_capacity.asp>

[7] Sorensen, J.N. and A. Myken, "Unsteady actuator disc model for horizontal axis wind turbines," J. Wind Engineering and Industrial Aerodynamics, Vol. 39, pp. 139-149, 1992.

[8] Ohya, Y., Karasudani, T., Sakurai, A., Abe, Ken-ichi, and M. Inoue, "Development of a shrouded wind turbine with a flanged diffuser," J. Wind Engineering and Industrial Aerodynamics, Vol. 96, pp. 524-539, 2008.

[9] Salim, M.S., and S.C. Cheah, "Wall y^+ Strategy for Dealing with Wall-bounded Turbulent Flows," Proceedings of the International MultiConference of Engineers and Computer Scientists 2009 Vol II IMECS 2009, March 18-20, 2009, Hong Kong.

[10] Wang, F., Bai, L., Fletcher, J., Whiteford, J. and D. Cullen. "The methodology for aerodynamic study on a small domestic wind turbine with scoop." J. Wind Engineering and Industrial Aerodynamics, Vol. 96, pp. 1-24, 2008.

[11] Bardina, J.E.; Huang, P.G., and T.J. Coakley.: Turbulence Modeling Validation, Testing, and Development. NASA TM-110446, Apr. 1997

[12] Muggli, F.A., Eisele, K., Casey, M.V., Gülich, J., and A. Schachenmann, "Flow Analysis in a Pump Diffuser – Part 2: Validation and Limitations of CFD for Diffuser Flows." J. Fluids Engineering, Vol. 119, 1997.

[13] Simpson, R.L., "Turbulent Boundary-Layer Separation." Ann. Rev. Fluid Mechanics, Vol. 21 pp. 205-34, 1989.

[14] Islam, M., David, S., Ting, K., and A. Fartaj, "Aerodynamic models for Darrieus-type straight-bladed vertical axis wind turbines," Renewable and Sustainable Energy Reviews, Vol. 12, No. 4, pp. 1087-1109, 2008.

[15] Dabiri, J.O., "Potential order-of-magnitude enhancement of wind farm power density via counter-rotating vertical-axis wind turbine arrays." J. Renewable Sustainable Energy 3, Article 043104, 2011.

[16] Antheaume, S., Maitre, T., and J. Achard, "Hydraulic Darrieus turbines efficiency for free fluid flow conditions versus power farms conditions," Renewable Energy, Vol. 33, pp. 2186-2198, 2008.

[17] Beri, H., and Yingxue Yao, "Numerical Simulation of Unsteady Flow to Show Self-starting of Vertical Axis Wind Turbine Using Fluent," J. Applied Sciences, 11: 962-970, 2011.

[18] Sheldahl, R.E., and P.C. Klimas, "Aerodynamic Characteristics of Seven Symmetrical Airfoil Sections Through 180-Degree Angle of Attack for Use in Aerodynamic Analysis of Vertical Axis Wind Turbines," Technical Report – Sandia National Laboratories, SAND80-2114, 1981.

[19] Hameed, M. S., and S. K. Afaq, "Design and Analysis of a straight bladed vertical axis wind turbine blade using analytical and numerical techniques." Ocean Engineering, Vol. 57, 2013.

[20] Untaroiu, A., Wood, H.G., Allaire, P.E., and R.J. Ribando, "Investigation of Self-Starting Capability of Vertical Axis Wind Turbines Using a Computational Fluid Dynamics Approach," J. Solar Energy Engineering. Vol. 133, 2011.

[21] Maître, T., Amet, E., and C. Pellone, "Modeling of the flow in a Darrieus water turbine: Wall grid refinement analysis and comparison with experiments," Renewable Energy, Vol. 51, pp. 497-512, 2013.

[22] Maughmer, M.D., and J.G. Coder, "Comparisons of Theoretical Methods for Predicting Airfoil Aerodynamic Characteristics," Subcontract for RDECOM, University Park, PA, 2010.

[23] Fish, F.E., Weber, P.W., Murray, M.M., and L.E. Howle, "The Tubercles on Humpback Whales' Flippers: Application of Bio-Inspired Technology." Integrative and Comparative Biology, Vol. 51, No. 1, pp. 203-213, 2011. Doi: 10.1093/icb/icr016

[24] Dahl, K.S., and P. Fuglsang, "Design of the Wind Turbine Airfoil Family RISO-A-XX," Riso National Laboratory, Roskilde, Denmark, RISO-R-1024(EN), 1998.

[25] Miklosovic, D.S., Murray, M.M., Howle, L.E., and F.E. Fish, "Leading-edge tubercles delay stall on humpback whale (Megaptera novaeangliae) flippers." Physics of Fluids. Vol. 16, No. 5, 2004, DOI: 10.1063/1.1688341

[26] Swanson, T. and K.M. Isaac, "Biologically Inspired Wing Leading Edge for Enhanced Wind Turbine and Aircraft Performance," Proceedings from the AIAA Theoretical Fluid Mechanics Conference, 27-30 June 2011, Honolulu, Hawaii.

[27] Abbot, H.A., and A.E. von Doenhoff, "Theory of wind sections: including a summary of airfoil data" ebook. Courier Dover Publications, Technology & Engineering, 1959.

[28] Kishore R. A., Coudron T., Priya S., "Small-scale wind energy portable turbine (SWEPT)" J. Wind Eng. Ind. Aerodyn. Vol. 116 pp. 21–31, 2013.

[29] JMP®, Statistics and Graphics Guide, Chapter 15: Profiling. JMP®, 2007.

[30] Renewable Devices, "accessible renewable energy," accessed 10 April 2013, < http://renewabledevices.com/rd-swift-turbines/features/ >

[31] LaMonica, M., "Small wind: Marquiss Wind Power gets funding for 'Ducted Wind Turbine,' cnet.com 25 January 2008. , http://news.cnet.com/8301-11128_3-9858643-54.html >

[32] Ragheb, M. Vertical Axis Wind Turbines. 8/1/2011

[33] Thomsen, Jesper, "VAWT Drawing," February 2013.

[34] Camporeale, S.M., and V. Magi, "Streamtube model for analysis of vertical axis variable pitch turbine for marine currents energy conversion," Energy Conversion & Management, Vol. 41, pp. 1811-1827, 2000.

[35] Hill, N., Dominy, R., Ingram, G, and J. Dominy, "Darrieus turbines: The physics of self-starting," Proceedings of the Institution of Mechanical Engineers, Part A: Journal of Power and Energy, Vol. 223, No. 21, 2009. DOI: 10.1243/09576509JPE615.

[36] Mukinović, M., Brenner, G., and A. Rahimi, "Analysis of Vertical Axis Wind Turbines," Numerical & Experimental Fluid Mechanics VII. 112, 2010.

[37] Olsman, W.F.J, Willems, J.F.H, Hirschberg, A., Colonius, T., and R.R. Trieling, "Flow around a NACA0018 airfoil with a cavity and its dynamical response to acoustic forcing," Exp. Fluids, Vol. 51, pp. 493-509, 2011.

[38] Timmer, W.A., "Two-dimensional low-Reynolds number wind tunnel results for airfoil NACA 0018," Wind Engineering Vol. 32, No. 6 pp. 525-537, 2008.

[39] Sabaeifard, P., Razzaghi, H., and A. Forouzandeh, (2012) "Determination of Vertical Axis Wind Turbines Optimal Configuration through CFD Simulations," 2012 International Conference on Future Environment and Energy, Vol. 28, pp. 109 – 113, 2012.

[40] Sharman, H., "Why wind power works for Denmark," Proceedings of ICE, Civil Engineering, Vol. 158, pp. 66-72, Paper 13663, 2005.

[41] Migliore, P.G., and J.R. Fritschen, "Darrieus Wind Turbine Airfoil Configurations: A Subcontract Report," Melior Corporation, Davis, California, Prepared for the U.S. Department of Energy under Contract No. EG-77-C-01-4042, 1982.

[42] Paraschivoiu, I., "Predicted and Experimental Aerodynamic Forces on the Darrieus Rotor," J. Energy, Vol 7, No. 6, pp. 610-615, 1983.

[43] Quinn, S., and W. Gaughran, "Bionics – An inspiration for intelligent manufacturing and engineering," Robotics and Computer-Integrated Manufacturing, Vol. 26, pp. 616-621, 2010.

[44] JMP, "JMP Design of Experiments (DOE)," JMP World Headquarters, SAS Institute Inc., 2007

[45] Munson, B. R., Young, D.F., and T.H. Okiishi, Fundamentals of Fluid Mechanics, 5th Edition, John Wiley & Sons, Inc., Hoboken, NJ, Ch. 8, 2006.

[46] ANSYS, ANSYS FLUENT Theory Guide, Release 14.0, ANSYS, Inc., Canonsburg, PA, November 2011.

[47] Aerospace and Ocean Engineering Department, Virginia Tech, "Virginia Tech Stability Wind Tunnel," www.aoe.vt.edu

[48] Weber, P.W., Howle, L.E., Murray, M.M., and D.S. Miklosovic, "Computational Evaluation of the Performance of Lifting Surfaces with Leading-Edge Protuberances," J. Aircraft, Vol. 48, No. 2, 2011. DOI: 10.2514/1.C031163

[49] Pedro, H.T.C., and M.H. Kobayashi, "Numerical Study of Stall Delay on Humpback Whale Flippers," 46th AIAA Aerospace Sciences Meeting and Exhibit, AIAA Paper 2008-0584, Reno, NV, 2008.

[50] Howell, R., Qin, N., Edwards, J., and Durrani, N., "Wind Tunnel and Numerical Study of a Small Vertical Axis Wind Turbine," Renewable Energy, Vol. 35, pp. 412–422., 2009.

APPENDIX A

TABLE A.1 DIFFUSER PARAMETER COMBINATIONS AND THEIR VELOCITY AMPLIFICATION AND SEPARATION CHARACTERISTICS

L_{in} (m)	θ_{in} (˚)	L_{out} (m)	Θ_{out} (˚)	Velocity Amplification Factor	Separation Characteristics
0.1	50	0.425	0	1.30	Does not separate
0.1	30	0.85	0	1.21	Does not separate
0.1	50	0.85	0	1.30	Does not separate
0.1	10	1.8375	0	1.29	Does not separate
0.1	50	1.8375	0	1.22	Does not separate
0.1	40	2.125	0	1.32	Does not separate
0.1	20	0.425	10	1.35	D
0.1	40	0.425	10	1.33	D
0.1	20	0.85	10	1.42	D
0.1	30	1.5	10	1.48	D
0.1	50	1.5	10	1.45	D
0.1	10	2.125	10	1.47	TD
0.1	50	2.125	10	1.55	D
0.1	20	0.425	15	1.33	D
0.1	20	0.85	15	1.37	D
0.1	50	1.5	15	1.41	D
0.1	10	1.8375	15	1.51	TD
0.1	30	1.8375	15	1.51	TD
0.1	20	2.125	15	1.45	D
0.1	40	2.125	15	1.44	D
0.1	10	0.425	18	1.26	D
0.1	40	0.85	18	1.28	D
0.1	50	1.5	18	1.48	TD
0.1	30	1.8375	18	1.43	D
0.1	20	2.125	18	1.55	D
0.1	30	0.425	2	1.35	Does not separate
0.1	30	0.85	2	1.38	Does not separate
0.1	40	1.5	2	1.39	Does not separate
0.1	10	1.8375	2	1.34	Does not separate
0.1	50	1.8375	2	1.38	Does not separate
0.1	20	2.125	2	1.35	Does not separate
0.1	30	0.425	20	1.34	D
0.1	50	0.425	20	1.27	D
0.1	40	0.85	20	1.40	D

0.1	50	0.85	20	1.30	D
0.1	10	1.5	20	1.29	D
0.1	20	1.5	20	1.35	D
0.1	20	1.8375	20	1.46	TD
0.1	40	2.125	20	1.36	TD
0.1	50	0.425	4	1.39	Does not separate
0.1	10	0.85	4	1.38	D
0.1	30	1.5	4	1.52	Does not separate
0.1	50	1.5	4	1.52	Does not separate
0.1	20	1.8375	4	1.50	Does not separate
0.1	40	1.8375	4	1.54	Does not separate
0.1	10	2.125	4	1.49	ITD
0.1	20	2.125	4	1.43	Does not separate
0.1625	20	0.425	0	1.33	Does not separate
0.1625	40	0.85	0	1.28	Does not separate
0.1625	20	1.5	0	1.26	Does not separate
0.1625	50	1.5	0	1.27	Does not separate
0.1625	30	1.8375	0	1.26	Does not separate
0.1625	10	2.125	0	1.18	Does not separate
0.1625	10	0.85	10	1.38	D
0.1625	20	1.5	10	1.56	D
0.1625	40	1.5	10	1.51	D
0.1625	50	1.8375	10	1.49	D
0.1625	30	2.125	10	1.36	D
0.1625	20	0.425	15	1.38	D
0.1625	30	0.425	15	1.39	D
0.1625	40	0.425	15	1.30	D
0.1625	30	0.85	15	1.45	D
0.1625	10	1.5	15	1.51	D
0.1625	40	1.8375	15	1.46	D
0.1625	50	2.125	15	1.46	TD
0.1625	10	0.425	18	1.32	D
0.1625	20	0.425	18	1.37	D
0.1625	50	0.85	18	1.31	D
0.1625	30	1.5	18	1.50	D
0.1625	50	1.5	18	1.32	D
0.1625	10	1.8375	18	1.40	D
0.1625	40	2.125	18	1.63	D
0.1625	50	2.125	18	1.49	D
0.1625	30	0.425	2	1.37	Does not separate
0.1625	50	0.425	2	1.31	Does not separate

0.1625	20	0.85	2	1.36	Does not separate
0.1625	40	0.85	2	1.38	Does not separate
0.1625	20	1.5	2	1.36	Does not separate
0.1625	30	1.8375	2	1.46	Does not separate
0.1625	10	2.125	2	1.34	Does not separate
0.1625	40	0.425	20	1.30	D
0.1625	20	0.85	20	1.40	D
0.1625	30	1.5	20	1.42	D
0.1625	40	1.8375	20	1.39	TD
0.1625	20	2.125	20	1.44	D
0.1625	50	2.125	20	1.46	TD
0.1625	40	0.425	4	1.40	Does not separate
0.1625	10	0.85	4	1.41	Does not separate
0.1625	50	0.85	4	1.45	ITD
0.1625	10	1.5	4	1.46	Does not separate
0.1625	20	1.8375	4	1.52	Does not separate
0.1625	30	1.8375	4	1.54	Does not separate
0.325	10	0.85	0	1.27	Does not separate
0.325	30	1.5	0	1.23	Does not separate
0.325	40	1.5	0	1.14	Does not separate
0.325	20	1.8375	0	1.30	Does not separate
0.325	50	2.125	0	1.16	Does not separate
0.325	10	0.425	10	1.47	Does not separate
0.325	40	0.425	10	1.22	D
0.325	30	0.85	10	1.70	Does not separate
0.325	50	0.85	10	1.13	TD
0.325	20	1.5	10	1.75	D
0.325	10	1.8375	10	1.59	D
0.325	40	1.8375	10	1.51	D
0.325	20	2.125	10	1.85	D
0.325	50	0.425	15	1.12	D
0.325	40	0.85	15	1.50	TD
0.325	20	1.5	15	1.54	D
0.325	50	1.5	15	1.43	TD
0.325	20	1.8375	15	1.57	D
0.325	10	2.125	15	1.55	D
0.325	30	2.125	15	1.60	D
0.325	30	0.425	18	1.36	D
0.325	30	0.85	18	1.44	D
0.325	40	0.85	18	1.48	TD
0.325	10	1.5	18	1.48	D

0.325	20	1.8375	18	1.54	D
0.325	40	0.425	2	1.15	Does not separate
0.325	50	0.85	2	1.19	Does not separate
0.325	10	1.5	2	1.34	Does not separate
0.325	10	1.8375	2	1.34	Does not separate
0.325	30	2.125	2	1.40	Does not separate
0.325	40	2.125	2	1.43	Does not separate
0.325	20	0.425	20	1.42	D
0.325	10	0.85	20	1.45	D
0.325	40	1.5	20	1.35	D
0.325	30	1.8375	20	1.46	D
0.325	10	2.125	20	1.50	D
0.325	50	2.125	20	1.36	D
0.325	40	0.425	4	1.24	Does not separate
0.325	20	0.85	4	1.45	Does not separate
0.325	30	1.5	4	1.53	Does not separate
0.325	50	1.8375	4	1.57	ITD
0.325	30	2.125	4	1.56	Does not separate
0.65	30	0.425	0	1.12	Does not separate
0.65	40	0.425	0	1.21	Does not separate
0.65	20	0.85	0	1.15	Does not separate
0.65	10	1.5	0	1.24	Does not separate
0.65	50	1.8375	0	1.07	Does not separate
0.65	30	2.125	0	1.18	Does not separate
0.65	20	0.425	10	1.45	Does not separate
0.65	50	0.425	10	1.19	D
0.65	40	0.85	10	1.41	Does not separate
0.65	10	1.5	10	1.77	D
0.65	30	1.8375	10	1.98	Does not separate
0.65	50	2.125	10	1.39	D
0.65	10	0.85	15	1.53	D
0.65	50	0.85	15	1.07	D
0.65	30	1.5	15	1.50	D
0.65	40	1.5	15	1.21	TD
0.65	20	1.8375	15	1.72	D
0.65	50	1.8375	15	1.20	D
0.65	30	2.125	15	1.62	D
0.65	40	0.425	18	1.07	D
0.65	10	0.85	18	1.50	D
0.65	20	1.5	18	1.80	D
0.65	40	1.5	18	1.25	TD

0.65	20	1.8375	18	1.59	D
0.65	50	1.8375	18	1.22	D
0.65	10	2.125	18	1.58	D
0.65	30	2.125	18	1.49	TD
0.65	20	0.425	2	1.19	Does not separate
0.65	10	0.85	2	1.35	Does not separate
0.65	50	1.5	2	1.18	Does not separate
0.65	20	1.8375	2	1.44	Does not separate
0.65	40	1.8375	2	1.27	Does not separate
0.65	30	2.125	2	1.30	Does not separate
0.65	10	0.425	20	1.45	D
0.65	20	0.85	20	1.48	D
0.65	30	0.85	20	1.44	D
0.65	50	1.5	20	1.15	D
0.65	10	1.8375	20	1.56	D
0.65	10	0.425	4	1.07	Does not separate
0.65	30	0.85	4	1.28	Does not separate
0.65	20	1.5	4	1.55	Does not separate
0.65	50	1.5	4	1.28	Does not separate
0.65	40	2.125	4	1.41	Does not separate
0.65	50	2.125	4	1.47	D

APPENDIX B

EVALUATION OF NACA 0018 AIRFOIL USING TWO EQUATION TURBULENCE MODELS

The NACA 0018 airfoil has been evaluated using many turbulence models for this research. Significant ranges of angles of attack were tested using the k-ε RNG and SST k-ω two-equation turbulence models and the data is presented in Tables B.1 and B.2. The Reynolds number for both sets of simulations is 40,000.

Table B.1 Lift and Drag Comparisons Using the k-ε RNG Model with Scalable Wall Functions

Angle of Attack	Drag Coefficient	Tabulated Data (18)	Percent Error	Lift Coefficient	Tabulated Data (18)	Percent Error
3	0.0212	0.0225	6%	0.0716	0.2688	73%
4	0.0223	0.0235	5%	0.0943	0.3495	73%
5	0.0239	0.0247	3%	0.1156	0.4117	72%
6	0.0257	0.0263	2%	0.1355	0.4573	70%
10	0.1152	0.062	86%	0.7457	0.2108	254%
15	0.1813	0.177	2%	0.7537	0.0889	748%

Table B.2 Lift and Drag Comparisons Using the k-ω SST Model

Angle of Attack	Drag Coefficient	Tabulated Data (18)	Percent Error	Lift Coefficient	Tabulated Data (18)	Percent Error
0	0.0447	0.0214	109%	0.0157	0	0.0157*
3	0.0464	0.0225	106%	0.2387	0.2688	11%
4	0.0468	0.0235	99%	0.3074	0.3495	12%
5	0.0487	0.0247	97%	0.3675	0.4117	11%
6	0.0520	0.0263	98%	0.4557	0.4573	0%
10	0.0853	0.062	38%	0.5867	0.2108	178%
15	0.1536	0.177	13%	0.5671	0.0889	538%

*The absolute error is presented since the standard error calculation would require division by zero.